Landslides (2019) 16:2127–2150
DOI 10.1007/s10346-019-01217-4
Received: 15 September 2018
Accepted: 31 May 2019
Published online: 28 June 2019

Benjian Song · Yuanfang Cheng · Chuanliang Yan · Zhongying Han · Jiping Ding · Yang Li · Jia Wei

Influences of hydrate decomposition on submarine landslide

Abstract Natural gas hydrate reservoirs on the sea floor have characteristics of a shallow overburden depth, weakened rock formation, and easy deformation. Thus, the mining of hydrate may cause geological disasters such as submarine landslides. To clearly learn about the failure process of submarine landslides induced by hydrate decomposition and influence the laws of various factors on submarine slope stability, this study established a thermal-fluid-solid-stress coupling model for hydrate. In combination with a strength reduction method, submarine slope stability in the mining of hydrates was analyzed. By utilizing the orthogonal experimental design method, this study analyzed the influence laws of these factors, including the hydrate decomposition range, submarine slope angle, overburden depth of hydrates, thickness of hydrate layers, seawater depth, and initial hydrate saturation on submarine slope stability, and evaluated the sensitivity to these factors. The result shows that hydrate mining may result in settlement of the seafloor and slippage of submarine sedimentary layers to the mining center, thus probably inducing submarine landslides. According to the significance of influences on submarine slope stability, the factors were ranked in descending order as follows: submarine slope angle, hydrate decomposition scale, thickness of hydrate layer, overburden depth of hydrates, initial saturation of hydrate layer, and seawater depth. Among the above factors, except for the overburden depth of hydrates and the seawater depth, the increases of which promoted submarine slope stability, the increase in the values of the other factors reduced submarine slope stability to different degrees. Therefore, in the mining of hydrates, the effects of each factor on submarine slope stability should be evaluated comprehensively to prevent disasters such as submarine landslides.

Keywords Gas hydrate · Depressurization · Numerical simulation · Sensitivity evaluation · Strength reduction method · Orthogonal design

Introduction

Natural gas hydrate is a crystalline solid similar to ice that is formed by natural gas and water at low temperature and high pressure (Almenningen et al. 2016). Hydrate distributes mainly in permafrost and shallow sedimentary layers of deep water (Chong et al. 2017). Due to its characteristics such as large reserves (energy stored in hydrate is twice conventional fossil energy), wide distribution, low pollution, and high-energy density, hydrate is considered an important alternative energy source for the future (Lee and Holder, 2001; Yan et al. 2017; Wang et al. 2019).

In view of hydrate mining, five methods (i.e., depressurization, thermal stimulation, chemical injection, carbon dioxide replacement, and solid fluidization) have been mainly proposed at present (Jin et al. 2016; Bhade and Phirani 2015; Zhou et al. 2018). To achieve the commercial mining of hydrate as soon as possible, a large number of laboratory and field experiments have been conducted. In 2007, pilot mining of hydrate using a depressurization method was conducted in the onshore well of Mallik 2L-38 in Canada and was terminated 60 h afterwards due to sand production. In 2008, after taking sand control measures, gas production on six consecutive days was 2000–4000 m^3, succeeding in pilot mining (Yamamoto and Dallimore, 2008). Furthermore, in 2013, a pilot mining experiment of submarine hydrate using a depressurization method was first carried out in Nankai Trough in Japan, and the cumulative gas production for 6 days reached 12,000 m^3, when the mining was forced to stop because of serious sand production (Yamamoto et al. 2014). In 2017, by also using the depressurization method for mining hydrate in the Shenhu Sea area in the South China Sea, the cumulative gas production for 60 consecutive days was more than 300,000 m^3 (Chen et al. 2018a, b). Based on the above field experiments, it is preliminarily that the depressurization method is effective and feasible for the recovery of hydrate (Nair et al. 2018). Considering economic costs, thermal stimulation is not suitable to be used as a dominant method for the large-scale development of hydrate, while thermal stimulation can be used as a supplementary measure to promote hydrate decomposition (Chen et al. 2018a, b). Due to the mechanism of action, decomposition efficiency and economic costs, the application of the chemical injection method and carbon dioxide replacement method is limited, and the two methods still remain in laboratory research at present (Moridis et al. 2007; White et al. 2011; Jin et al. 2018). In addition to the four conventional methods described above, the solid fluidization method was also used for mining submarine hydrate in the South China Sea in 2017, where the gas production was low (Zhou et al. 2018).

In particular, when the hydrate zone is in a submarine slope, hydrate decomposition can significantly decrease submarine slope stability and cause large-scale submarine landslides (Sultan et al. 2004; Kukowski et al. 2010; Micallef et al. 2012; Mountjoy and Micallef, 2012; Pedley et al. 2010). For instance, the second stage of the Storgga landslide, the largest known submarine landslide was mainly induced by hydrate decomposition (Bondevik et al. 2012). A massive landslide on the continental slope near the Gisborne Coast, as well as the Agadir Basin landslide, Amazon landslide, and Cape Blanc landslides, has a certain relationship with hydrate decomposition (Hunt, 2012; Mountjoy et al. 2009; Maslin et al. 2005; Wien et al. 2007).

The stability of submarine slope containing hydrates is affected by several factors, such as the depth of overlying seawater, overburden depth and thickness of hydrate layers, hydrate saturation, overburden depth of hydrate, slope angle, and hydrate development (Sultan et al. 2004, Sultan, 2007; Xu and Germanovich 2006; Wei et al. 2019). The view that hydrate decomposition on the slope reduces submarine slope stability and even results in submarine landslides is widely

accepted. However, at present, there is no systematical research on how to characterize submarine slope stability, dynamic process of submarine landslides caused by hydrate decomposition, and influence laws of various factors on submarine slope stability. By taking submarine slope containing hydrate in Shenhu sea area in the South China Sea as the research object, secondary development was conducted based on finite element software ABAQUS. By combining strength reduction method, this study simulated the whole failure process of submarine slopes caused by the mining of hydrate by using depressurization method in horizontal wells. Moreover, by employing the orthogonal experimental design method, this research analyzed influence laws of six factors, i.e., submarine slope angle, mining degree of hydrates, overburden depth of hydrates in the formation, thickness of hydrate layers, seawater depth, and initial saturation of hydrates on stability of the slope containing hydrates.

Mathematical model

Hydrate decomposition kinetic model

Natural gas hydrates are formed from alkanes and water under low temperature and high-pressure conditions. The most widely distributed and studied hydrates are methane hydrates. For methane hydrate, its dissociate equation can be described as follows (Moridis 2002):

$$CH_4 \cdot nH_2O + \text{heat} \leftrightarrow CH_4(\text{gas}) + nH_2O(\text{liquid})$$

where the range of n is 5.5–6. Here, we consider that n is equal to 6. Hydrate dissociation is an endothermic reaction. The reaction heat is approximately 53 to 58 kJ/mol (Hu et al. 2017).

The phase boundary of methane hydrate can be modified according to the following equation (Kamath 1998):

$$P_{eq} = \exp\left(e_1 - \frac{e_2}{T}\right)$$

where P_{eq} is the phase equilibrium pressure at T temperature, and $e_1$and e_2 are regression parameters. For the different kinds of hydrates, the values are different. When $T > 0$ °C, e_1=39.08 and $e_2 = 8533$.

The kinetics of hydrate decomposition are affected by many factors. According to the research results of Sun et al., the kinetics are simplified to the functions of pressure, temperature, permeability, effective porosity, and time (Sun and Mohanty 2006; Gulbrandsen and Svartås 2017). The hydrate dissociation rate, gas generation rate, water generation rate, and reaction absorption heat rate can be described as follows:

$$-g^h = M_h k_{\text{reac}} \Gamma_r A_s \left(P_{eq} - f_g\right)$$

$$g^g = g^h \frac{M_g}{M_h}$$

$$g^w = n \times g^h \frac{M_w}{M_h}$$

$$A_s = \sqrt{\frac{\phi_e^3}{2k}} \quad \Gamma_r = \left(s_g s_w s_h\right)^{2/3}$$

$$h_a = h_r \frac{g^h}{M_h}$$

where g^h(kg/m^{3}s) is the hydrate assumption rate, g^g(kg/m^{3}s) is the gas generation rate, and g^w(kg/m^{3}s) is the water generation rate. M_g is the gas relative molecular mass, where we considered the gas is pure methane. M_h is the hydrate relative molecular mass. M_w is the water relative molecular mass. k_{reac}(mol/m^{2}Pas) is the kinetic constant for hydrate dissociation. f_g(Pa) is the gas fugacity calculated using the Peng-Robinson EoS for methane gas, and A_s(m^2/m^3) is the total surface area between hydrate particles and the surrounding phases. Γ_r is the ratio of the active reaction surface to the total surface area. A_s and Γ_r are modeled using correlations proposed by Sun and Mohanty (Sun and Mohanty 2006). The Γ_r considers that the hydrate growth that the template provides by the hydrate phase is fundamental, where k(md) is the permeability of porous media, which is related to the initial saturation of hydrates and the degree of hydrate decomposition. s_g is the gas saturation. s_w is the water saturation. s_h is the hydrate saturation. h_a(10^{3}kJ/m^{3}s) is the reaction absorption heat rate. h_r is the hydrate dissociation reaction heat; here, $h_r = 53$ kJ/mol. By editing the HETVAL subroutine in ABAQUS, the reaction heat of the hydrate decomposition can be input into the numerical calculation.

The permeability of the hydrate formation is affected by the hydrate saturation because the hydrate does not participate in multiphase flow in the pores and is an ineffective pore fraction. Therefore, in the hydrate permeation analysis, the ratio of the volume occupied by the hydrate and the fluid (including gas) in the formation to the volume of the formation is defined as the formation porosity, and the ratio of the volume occupied by the fluid (including the gas) to the total volume of the formation is defined as effective porosity. After the hydrate is decomposed, the effective porosity increases, and the formation permeability increases. When the initial hydrate saturation is at a high level, there is a difference of one to two orders of magnitude in the formation permeability before and after hydrate decomposition (Soldi et al. 2017; Katagiri et al. 2017).

$$k = k_o \left[\frac{\phi_e}{\phi_o}\right]^5 \times \left[\frac{1-\phi_o}{1-\phi_e}\right]^2$$

$$\phi_e = \phi_o \cdot \left(s_g + s_w\right)$$

k is the hydrate formation permeability. k_o is the formation initial permeability. ϕ_e is the effective porosity. ϕ_o is the formation porosity.

In ABAQUS, the comprehensive permeability of the porous medium can be corrected according to the water phase saturation defined in subroutine, as shown in the following formula.

$$\hat{k} = k_s k_0 \left[\frac{\phi_e}{\phi_0}\right]^5 \times \left[\frac{1-\phi_0}{1-\phi_e}\right]^2$$

$\hat{k}$ is the comprehensive permeability of the porous medium. k_s provides the dependency on saturation, with $k_s = 1.0$ is the permeability of the fully saturated medium. The function k_s can be defined by default in ABAQUS as $k_s = s_w^3$.

All of the above equations can be coded into the USDFLD subroutine on the basic of ABAQUS via Fortran. Finally, the relationship between hydrate saturation and formation temperature as well as pressure and physical parameters and time is established to achieve the numerical simulation of hydrate decomposition dynamics and lay the foundation for subsequent analysis.

Hydrate sediment geomechanical evolving model

The dynamic change in the mechanical parameters during hydrate decomposition is a difficult point in the hydrate formation simulation analysis. The strength of the hydrate is higher than that of the sediment, and the hydrate has a cement-like effect that enhances the total strength of the hydrate sediment (Sánchez et al. 2017). When the hydrate is decomposed into gas and water, the strength of the formation will be reduced under the influence of two aspects (Lin et al. 2017). First, the formation loses the support and cementation effect provided by the hydrate. The second aspect is the destruction of the skeletal structure caused by a large amount of gas generated by the decomposed hydrate. In addition, many triaxial experiments confirm that the stress-strain relationship of a hydrate sediment is not expressed as elastic behavior (Ling et al. 2014). To describe the mechanical properties of hydrates, numerous on-site and indoor experiments have been carried out, and many constitutive equations have been obtained. For example, Miyazaki et al. proposed a nonlinear elastic for hydrate-bearing sediment based on the Duncan-Chang model (Miyazaki et al. 2012). The Mohr-Coulomb model used to describe the mechanical behavior of rock and the Cam-Clay model used to describe the behavior of soil mechanics are modified to describe the mechanical properties of hydrate formations (Sultan and Garziglia 2011).

Compared with several constitutive hydrate sediment models, the model we chose was established by Pinket et al. (Pinkert and Grozic 2014). This constitutive model is based on the Mohr-Coulomb model, which was developed according to nonlinear theory and the failure criterion in the MC mode. The hydrate saturation is considered. The prediction of this model is in accordance with the Miyazaki et al. (2011) experimental data. In addition, all the variables can be set directly in ABAQUS. This model is shown as follows (Pinkert and Grozic 2014):

$$c = c_s + c_h = c_1\left(1 - e^{-\frac{\sigma_3'}{\sigma_t'}}\right) + c_2 s_h^{c_3}$$

$$\sin\phi = \sin\phi_s + \sin\phi_h = \sin\left(\delta_1 - \delta_2 \ln\left(\frac{\sigma_3'}{1_{\mathrm{MPa}}}\right)\right) + \delta_3 s_h\left(1 - e^{-\frac{\gamma}{\delta_4}}\right)$$

$$E = E_s + E_h = e_1\left(\frac{\sigma_3'}{1_{\mathrm{MPa}}}\right)^{e_2} + e_3 s_h$$

where the c_s and c_h are the cohesion of sand and hydrate. σ_t' increases with failure. c_1 depends on σ_t'. ϕ is the dilation angle, ϕ_s is the dilation angle of sand, and ϕ_h is the dilation angle of hydrate. δ_1 and δ_2 are constants that are governed by density and solid material, and δ_3 increases with dilation on account of the existence of hydrate. s_h is the saturation of the hydrate. σ_3' and δ_4 are constants that are associated with shear strain. γ is the internal shear strain. E is the comprehensive Young's modulus, and E_s and E_h are the Young's modulus associated with the sand and hydrate. c_2, c_3, e_1, e_2, and e_3 are constants. For different areas and blocks, there are different hydrate sediment skeleton coefficients (Yamamoto 2015). According to previous studies, the skeleton coefficient of the hydrate deposits in the Shenhu area of the South China Sea combined with the Pinket constitutive equation is shown in Table 1 (Pinkert and Grozic 2014; Chen et al. 2018a, b; Feng et al. 2015).

According to the above formula and parameters shown in Table 1, the relationship between hydrate bearing sediments strength and hydrate saturation is obtained, as shown in Fig. 1.

Submarine slope stability model

Strength reduction method based on ABAQUS

Traditional slope stability analysis methods mainly include limit analysis, limit equilibrium, and numerical calculation methods based on the finite element. With the development of computer technology and the finite element, the stability analysis method based on the stress field and the finite element strength reduction method are widely recognized and gradually become the development direction of slope stability analysis (Althuwaynee et al. 2018). The strength reduction factor F_r at the time of critical failure is the safety factor F_s of the slope (Chen et al. 2016). In this study, the finite element strength reduction method was adopted as the guiding method for slope stability analysis, and the safety degree was used to characterize the stability of the seabed slope.

The reduced shear strength parameters can be expressed as follows (Bru et al. 2018):

$$c_m = c/F_r$$

$$\phi_m = \arctan(\tan\phi/F_r)$$

where c_m and ϕ_m are the cohesion and friction angles required to maintain the balance that the soil actually exerts; F_r is the strength reduction factor.

ABAQUS is a general purpose finite element analysis software that analyzes fluid seepage and geomechanical problems in porous media and has been widely used in slope stability analysis in recent years (Kostov et al. 2015; Zhu et al. 2015; Guo et al. 2016; Li et al. 2018; Yan et al. 2018). ABAQUS can automatically increase the reduction factor, change the strength of the material, and, finally, get the reduction factor when the calculation is interrupted. On this basis, according to the slope instability criterion, the safety factor of the slope under this condition is determined, and the subsequent analysis is carried out according to the obtained results (Feng et al. 2018).

Table 1 Hydrate sediment skeleton coefficient

Parameter	Value	Unit	Parameter	Value	Unit
c_1	293	kPa	δ_3	0.22	
c_2	1960	kPa	δ_4	0.04	
c_3	1.7		e	2.72	
$\sigma_3^{'}$	1962	kPa	e_1	241,200	kPa
$\sigma_t^{'}$	382	kPa	e_2	0.642	
δ_1	0.4		e_3	450,000	kPa
δ_2	0.1		γ	9	

Slope instability criteria

According to the appropriate slope instability criteria, the safety factor of the slope can be determined. The criteria for slope instability also directly affect the understanding of slope stability and the accuracy of the strength reduction method. At present, there are several evaluation criteria for judging the critical damage of soil slopes (Masson et al. 2011):

1) Forming a continuous plastic penetration zone
2) Significant displacement occurring at the inflection point at the top of the slope
3) Calculation caused by large deformation of the model not converging and terminating

When the safety factor that is obtained is greater than 1, it indicates that there is no risk of landslide on the slope. When the safety factor is less than 1, it indicates that the slope will be unstable under natural conditions, and the risk of geological disaster needs to be evaluated.

Solution strategy in ABAQUS

Hydrate sediment is a typical porous media. This model is implemented in ABAQUS with a fully coupled solution approach. On the basis of the effect stress principle, the solution strategy is the following: (1) discretizing the porous media for equilibrium statement, (2) calculating the constitutive behavior in a porous medium of fluid and skeleton structure, (3) catching the continuity statement for the wetting liquid phase in a porous medium, (4) coupling the diffusion/deformation and heat transfer process. For such a solution strategy, many equations are needed which include effective stress principle, discretize equations, governing equation, continuity equation, constitute behaviors (liquid response equation and solid response equation), heat balance equation, and the heat conduction equation. Part of this equation can be referred in the Appendix in revised manuscript.

Numerical model

Site description

The Shenhu area is found in the northern slope of the South China Sea, where hydrates were successfully recovered more than 60 days

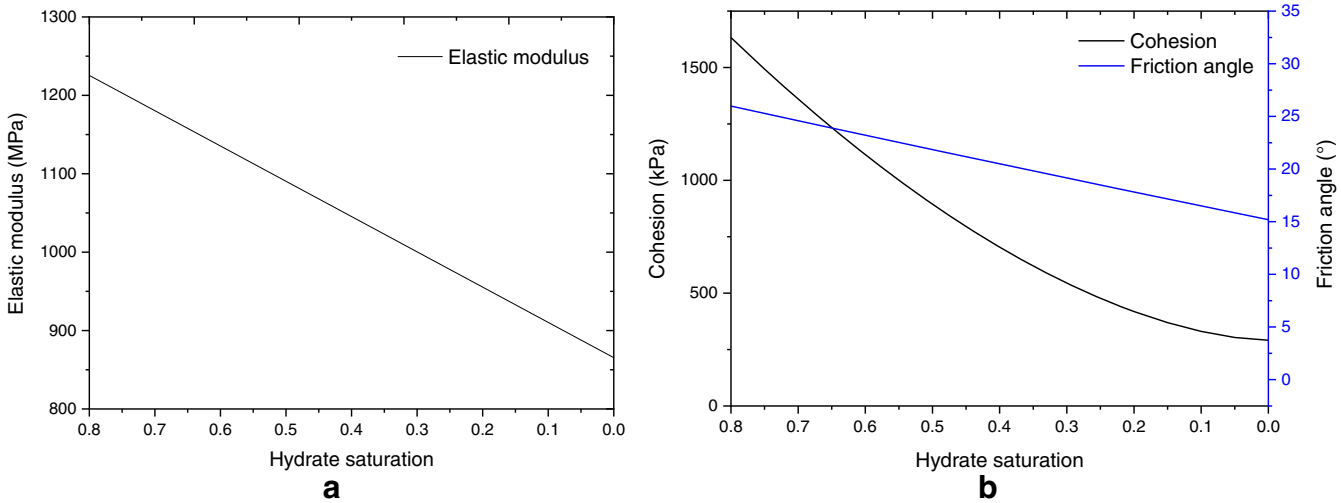

Fig. 1 The relationship between the hydrate bearing formation strength and hydrate saturation (a) the elastic modulus against hydrate saturation (b) the cohesion and internal friction angle against hydrate saturation.

in 2017 by the Chinese geological survey. This paper studies the background of hydrate mining in the slope area of the Shenhu Sea in the South China Sea with hydrate sediments. The average slope angle is approximately 3.3 to 3.6°, and the maximum angle reaches 25°. According to the samples from the Shenhu area, the temperature of the seabed is 2.3–3.7 °C, while the depth of the seawater is more than 1000 m. The stratum temperature gradient is 30–45 °C/km. According to the lithology logs at the Shenhu drill hole, the distance between the top surface of the hydrate sediment to the sea floor is approximately 50–350 m. The thickness of the hydrate sediment is estimated to be 10–120 m. The porosity of the hydrate sediment is 33–48%, while the hydrate saturation is greatly anisotropic in different areas, and the value is 0.2–0.76. Methane constitutes more than 96% of the hydrate decomposition products, while ethane and propane constitute the remaining parts (Li et al. 2010).

Numerical model establishment

Model sketch

The submarine slope model includes sedimentary layers not containing hydrate and containing hydrate reservoirs, and it is assumed that these two formations were homogeneous and isotropic materials. The depressurization method was used for mining hydrate in horizontal wells. In combination with the depressurization method of horizontal wells, the contact area between shaft and hydrate formation significantly increases, thus resulting in pressures in the shaft that are propagated in a larger area in the formation. This result brings greater safety risks while decomposing hydrate over a large range.

According to the above experimental schemes, the 3D model of a series of slopes containing hydrate was established by using ABAQUS software, and the sketch map of the model is shown in Fig. 2. The numerical model in a total length of 1600 m has a slope with a span of 1200 m, and there are horizontal submarine planes with a length of 200 m on the left and right sides. The maximum height of the model is 800 m, while the minimum height is adjusted according to the slope angle. As demonstrated in the figure, when the angle is 15°, the minimum height of the slope is $800 - 1200 \times \tan 15^\circ = 478.7(\mathrm{m})$. The hydrate-bearing zone is in the length of 800 m, and the right side is directly below the highest point of the slope. The overlaying sedimentary layers in the whole hydrate-bearing zone have the same thickness. The production well is a horizontal well passing through the whole model and located at the half-thickness depth of the hydrate layer.

Because slope heights are different, the seawater depth refers to the height of overlying seawater in the highest position of the model. In Fig. 2, the seawater depth in the model is 1300 m. Therefore, for experimental schemes under different slope angles at the same seawater depth, pore pressures applied on different models are unequal, causing calculation errors. In the subsequent analysis, the factor of the seawater depth needs to be set as the factor containing errors. In accordance with the set experimental schemes, these parameters such as slope angle, thickness of hydrate layers, overburden depth of hydrate layers, and seawater depth were adjusted, as well as the position of the well, to analyze slope stability under different slope conditions.

Model mesh and boundary conditions

Figure 3 shows the mesh of the numerical model. The blue area is the hydrate formation, and the other area is the sediment formation. The mesh of hydrate formations and the area connected to the hydrate layer were refined. The mesh near the horizontal well was a circular grid centered on the horizontal well, which is advantageous for the radial flow simulation around horizontal well. In the *y*-direction, the mesh seeds number is 8, and the total number of grids is 43,488. The mesh element type is coupled temperature-pore pressure provided by ABAQUS. Under this type, stress field-seepage field-temperature field can be simultaneously coupled and calculated.

The model considers the factors such as stress state and temperature-pressure environment of slope containing hydrates under real conditions. The upper and lower surfaces of the model are boundaries of fixed temperature and pore pressure, where the influences of vertical sections of the production well on the small ranges of formation are neglected. The whole model is homogeneous in the *y*-direction. Therefore, the displacements on the front and rear surfaces of the model in the *y*-direction are constrained. Because the left and right surfaces of the model are connected with the infinite formation, displacements of the left and right surfaces of the model in the *x*-direction are constrained (De Luca and Versace 2017). Similarly, the displacement of the lower surface of the model in the *z*-direction is limited. The wellhole was set as the pore pressure boundary with 9 MPa pressure in all cases. The whole model is affected by gravity, in situ stress, overlying seawater pressure, and pore pressure.

Numerical model parameters

For the model, we assume that the water temperature of the sea floor does not change with the seawater depth but remains at 2 °C and that the submarine geothermal gradient is 3.5 °C/100 m. Moreover, seawater density and pore water density in the formation are constants. The model simulated heat changes and influences on temperature fields in the formation caused by hydrate decomposition and regeneration when pore pressure in the formation changed. In addition, the changes in the pore pressures in the formation and fluid migration in the hydrate mining in the formation by using depressurization method were simulated. Seepage parameters and thermodynamic parameters in the model are shown in Table 2. The initial porosity of the model is 0.4, and the permeability of the formation without containing hydrate is 0.6 mD. The permeability in the formation containing hydrate is correlated with initial saturation and decomposition degree of hydrate. To reduce the impacts of initial permeability on the propagation of pore pressures, the initial permeability of hydrate layers is set to be a constant, 0.2 mD, and permeability after hydrate decomposition is calculated through the formula. The thermal parameters of the actual substance are more likely to have a relation with temperature. To reduce calculation, thermal conductivity is set as a constant in the model.

[d]Jin et al. (2016)

Solution process

According to the set experimental schemes, the numerical model was established by using ABAQUS. The seafloor settlement and slope slide occur with large deformation caused by hydrate decomposition. By turning on the Nlgeom (geometric nonlinearity)

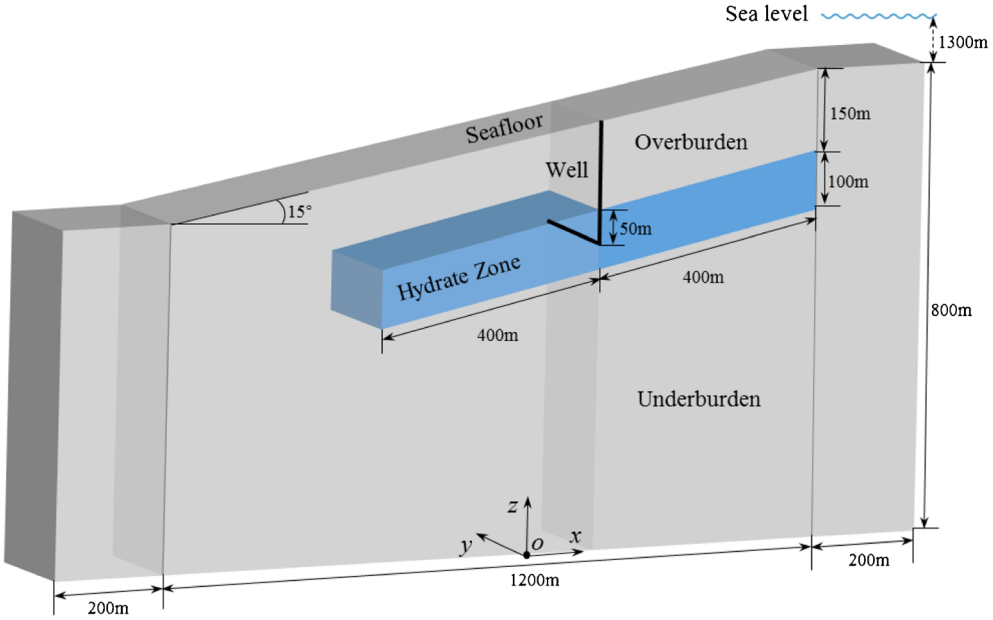

Fig. 2 Sketch map of the numerical model of submarine slope

in step manager process in ABAQUS, large deformation problems can be solved. The calculation process is divided into three steps, that is, the balance analysis of the in situ stress, hydrate decomposition analysis, and strength reduction analysis. The balance analysis of in situ stress aims to restore the original static state in the formation and eliminate the influences of in situ stress and gravity on model size to reach the actual state with stress and without strain in the formation. Then, the hydrate production was analyzed. The production of hydrate was accompanied by dynamic changes of all parameters including stress field, seepage field and temperature field, and the analysis did not stop until the scale of hydrate decomposition reached the requirements in the predetermined scheme. The last step is the strength reduction analysis. In the first step, the Nlgeom was turned off, and in next two steps, it was turned on. In accordance with the safety factor of submarine slopes obtained through the strength reduction analysis, the influence laws of each factor on submarine slope stability were evaluated.

Numerical simulation scheme

In this research, by utilizing the orthogonal experimental design method, the scheme of numerical simulation was designed. The orthogonal experimental design method is a scientific method that reasonably arranges experimental schemes by selecting a certain

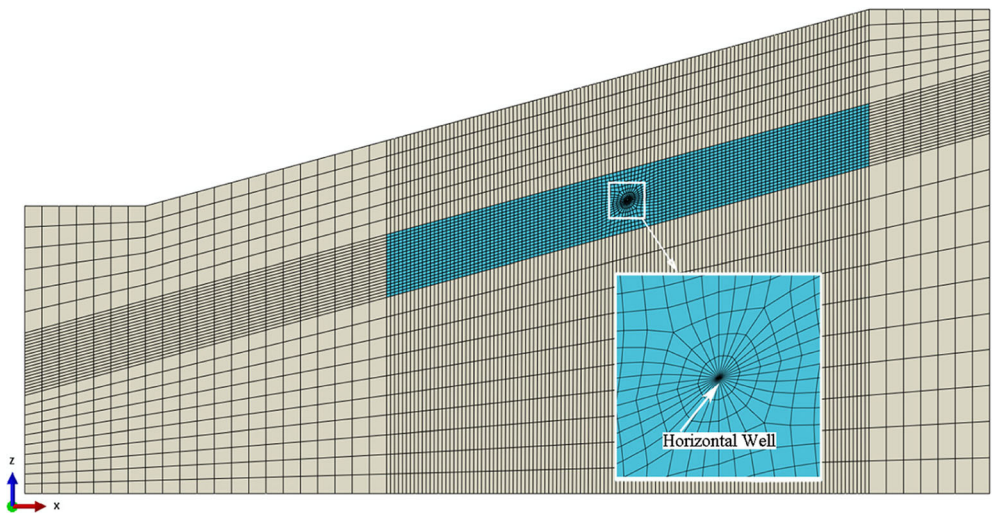

Fig. 3 Model meshing on the *x*-*z* plane

Table 2 Thermal-physical parameters of the formation

Parameter	Value	Parameter	Value
Porosity[a, b]	0.4	Water density[d]	1040 kg/m^3
Hydrate density[c]	920 kg/m^3	Water thermal conductivity[c]	3.0 W/m K
Hydrate thermal conductivity[c]	0.5 W/m K	Water specific heat	4.2 kJ/kg K
Hydrate specific heat[c]	2.1 kJ/kg K	Water saturation of Sand[d]	1
Rock grain density[a]	2600 kg/m^3	Water saturation of Hydrate sediment	1-s_h
Rock grain thermal conductivity[c]	1.0 W/m K	Sand instinct permeability[a, b]	0.6 mD
Rock grain specific heat[c]	1.0 kJ/kg K	Hydrate instinct permeability[a, b]	0.2 mD
Submarine water temperature[d]	2 °C	Geothermal gradient[d]	3.5 °C/100 m

[a] Zhang et al. (2010)

[b] Su et al. (2012)

[c] Moridis et al. (2008)

number of representative points from many experimental points through the created orthogonal design table. The advantages of the orthogonal experimental design are that the number of experimental schemes is greatly reduced, and a small number of representative experimental schemes can represent analysis results obtained through many experiments so that the designed schemes are more reasonable and efficient.

Orthogonal experimental design

The orthogonal experimental design involves three key elements, i.e., index, factor, and level. The purpose of the study is mainly to analyze the influence laws of each factor on submarine slope stability. Index refers to the safety factor of submarine slopes, and the research factors include the submarine slope angle, decomposition degree of hydrate caused by mining, depth of overlying seawater of slope containing hydrate, overburden depth of hydrate reservoirs, thickness of hydrate layers, and initial saturation of hydrate. According to the actual exploration data, five levels were determined for each factor. If the complete factorial experiment is utilized, the total number of experiments is $5^6 =$ 15,625, which is almost impossible to achieve in the time limit, and many experiments have no practical significance. In the orthogonal experimental design, by conducting only 25 independent experiments, one can characterize the influence of each factor on the indexes and evaluate the sensitivity of each factor.

The basic tool of the orthogonal experimental design method is the orthogonal design table in which factors and levels are key elements. Through the orthogonal design tables, data for factors influencing the results of the index combined at different levels are arranged scientifically and reasonably so that the experimental data are balanced and dispersed, meeting the requirements for comprehensively designing experiments and enabling one to research a problem effectively through the experimental schemes finally formed in the orthogonal table. In the orthogonal design table, L, n, S,and r indicate the code of the orthogonal design table, the times of the orthogonal experiments, the number of levels and the number of factors, respectively. The orthogonal table is generally represented by $L_n(S^r)$. By taking $L_{25}(5^6)$ as an example, it represents that 25 calculation schemes can be formed by the orthogonal table. Moreover, six factors are observed, and five levels are selected for each factor.

Factor sensitivity evolution in orthogonal experimental

Sensitively analysis is used for researching influence laws and degrees of change of different factors on indexes, further objectively evaluating the strength or degree of the sensitivity of factors. The estimated marginal mean analysis, range analysis, and variance analysis are three effective methods for analyzing the sensitivity of orthogonal experimental design results. For the estimated marginal mean analysis, it is used to analyze the influence trend of changes of a factor on experimental results by selecting a certain factor as the research subject while controlling other factors at the same level. In the analysis of submarine slope stability, the changes in the safety factor result from common effects of several factors. The estimated marginal mean analysis is equivalent to eliminating the influences of other variables on the safety factor to obtain the influence trend of a single factor on the safety factor. Through the range analysis, the degree of influence of each factor on the research into experimental indexes can be obtained. According to ranges of each influence factor, the sensitivities of factors are determined, while the significance of influences of each factor on the results of the experimental indexes cannot be determined. The variance analysis method can be used to study the significance of influences of each factor on indexes, thus accordingly determining the degree of influence of sensitivity. Such a method makes up for the deficiency of the range analysis. This study analyzed the sensitivity of the orthogonal experimental results by using the range and variance methods and compared the sensitivity results obtained by using these two methods. The above three analysis methods can be achieved in SPSS software.

Simulation scheme design

This study analyzed the influence laws of six influence factors, i.e., submarine slope angle, hydrate decomposition range caused by mining, the seawater depth of slope containing hydrate, overburden depth of hydrate reservoirs, thickness of hydrate

layers and initial saturation of hydrate on the submarine slope stability containing hydrates, and the sensitivities of the stability to these factors. In the analysis, factors that will significantly affect the decomposition rate of hydrates, such as time, production pressure, and temperature, were not taken into orthogonal analysis. This is because that these factors mainly affect the hydrate decomposition degree rather than directly affecting the slope stability. In different schemes, hydrate decomposition degrees are different at the same time, which denies the comparability of various schemes. Therefore, the range of the hydrate decomposition zone is used to describe the degrees of the hydrate decomposition. Specifically, it is defined as the ratio of total area of the hydrate decomposed zone to the height of hydrate decomposition region perpendicular to the slope direction. According to the geological characteristics of the Shenhu Sea in the South China Sea, based on relevant research and soil exploration data in this sea region, the value ranges of different influence factors were determined (Pinkert and Grozic 2014; Chen et al. 2018a, b; Feng et al. 2015; Gang, L. et al. 2010; Jin et al. 2018). To facilitate the design of experimental schemes and the resulting analysis, the above six influence factors were valued at five levels. In accordance with the $L_{25}(5^6)$ orthogonal experimental table, the orthogonal experimental schemes are presented in Table 3, where the specific factors and their values at different levels are displayed.

Results and conclusion

Stratum response to hydrate decomposition

In hydrate decomposition process, each physical property of the formation and stress changes dynamically. The description of the hydrate decomposition process is the basis of research analysis and influences on submarine slope stability. To intuitively characterize parameter setting of the model and the failure process of the slope in hydrate decomposition, by taking case-19 shown in Table 3 as an example, the dynamic response of the slope in hydrate decomposition and the failure process of the slope in reduction are illustrated.

Table 3 Orthogonal experimental design

	Slope angel (°)	Decomposition scale (m)	Overburden thickness (m)	Hydrate thickness (m)	Seawater depth (m)	Hydrate saturation
Case-1	10	0	50	20	1200	0.40
Case-2	10	50	100	40	1300	0.50
Case-3	10	150	150	60	1400	0.60
Case-4	10	250	200	80	1500	0.70
Case-5	10	350	250	100	1600	0.80
Case-6	12	0	100	60	1500	0.80
Case-7	12	50	150	80	1600	0.40
Case-8	12	150	200	100	1200	0.50
Case-9	12	250	250	20	1300	0.60
Case-10	12	350	50	40	1400	0.70
Case-11	15	0	150	100	1300	0.70
Case-12	15	50	200	20	1400	0.80
Case-13	15	150	250	40	1500	0.40
Case-14	15	250	100	60	1600	0.50
Case-15	15	350	50	80	1200	0.60
Case-16	18	0	200	40	1600	0.60
Case-17	18	50	250	60	1200	0.70
Case-18	18	150	50	80	1300	0.80
Case-19	18	250	100	100	1400	0.40
Case-20	18	350	150	20	1500	0.50
Case-21	20	0	250	80	1400	0.50
Case-22	20	50	50	100	1500	0.60
Case-23	20	150	100	20	1600	0.70
Case-24	20	250	150	40	1200	0.80
Case-25	20	350	200	60	1300	0.40

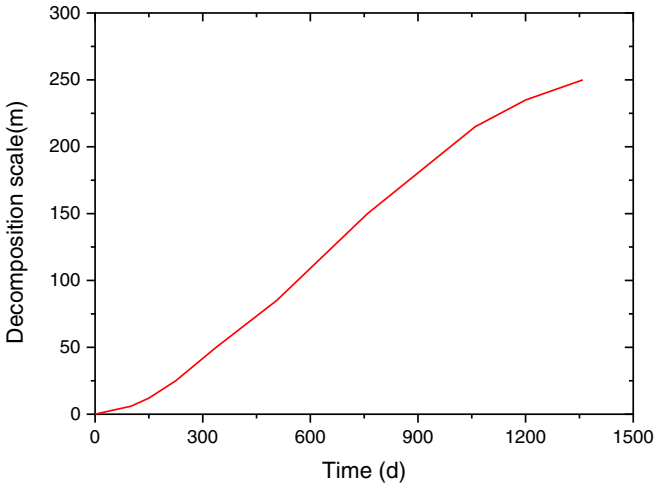

Fig. 4 Curve of the relationship between hydrate decomposition range and time

Hydrate decomposition process

In the depressurization production process, hydrates are decomposed from the wellbore to both sides. Under the control of temperature-pressure conditions of the formation and phase equilibrium conditions, the hydrate decomposition zone was shown as an irregular figure. The change curve of the hydrate decomposition range with time is demonstrated in Fig. 4. In the initial production stage of the hydrate, because of a small initial permeability and effective porosity of the hydrate-bearing formation, low liquid column pressures in the shaft could not rapidly propagate to the internal side of the formation. Therefore, in the early stage of the production, the hydrate decomposition scale increases relatively slowly. With the production of hydrate, porosity and permeability in the region after hydrate decomposition increase to some extent, thus promoting the propagation of low pressures and decomposition of hydrate and resulting in the gradually increasing speed of hydrate decomposition and maintenance of the stabilized decomposition for a period of time. With the increase in the hydrate decomposition range, the distance of pressure propagation increases, while the pressure drop at the leading edge of the hydrate decomposition decreases gradually, and the hydrate decomposition speed is reduced. Therefore, propagation speed at the leading edge of the hydrate decomposition shows a decreasing trend with the change in time.

In this scheme, the nephogram of hydrate saturation at different decomposition scales is shown in Fig. 5. The production pressure is 9 MPa, and the mining time from Fig. 5a to Fig. 5c is 337d, 760d, and 1354d, respectively. Due to the influences of geothermal gradients, phase equilibrium pressures of hydrate are high in the deep formation at a high temperature. Therefore, the decomposition speed of the hydrate to the depth of the formation is obviously faster than the decomposition speed of the hydrate to the upper formation and formation at the same depth. Furthermore, in hydrate decomposition, a transition zone was found near the leading edge of the hydrate decomposition, and some hydrates are decomposed in this zone. Under the above effects, the distribution of hydrate saturation shows triangular characteristics, as shown in Fig. 5 b and c.

Seepage characteristics response

Figure 6 demonstrates the dynamic response in the formation of the submarine slope when the hydrate decomposition range is 150 m and the corresponding time is 760d. As presented in Fig. 6a, the effective porosity of the zone where hydrates are decomposed is obviously larger than the porosity of the region with undecomposed hydrates. Furthermore, the permeability of hydrate layers is significantly higher than the permeability of the sedimentary layer, and the pressure drop centered on the wellbore propagates into the hydrate-bearing formation, further decomposing internal hydrates. As displayed in Fig. 6b, the range of the core pressure drop in the formation is approximately equal to the range of the hydrate decomposition zone. In addition, due to the low permeability of the sedimentary layers that do not contain hydrate, the propagation range of the low pressures in the sedimentary layers is limited. As shown in Fig. 6c, the distribution characteristics of the maximum principal stress in the formation are similar to those of hydrate saturation. After hydrate decomposition, the strength of the decomposition zone is rapidly reduced, and the corresponding effective stress decreases. The strength of the leading edge of the hydrate decomposition zone remains at a high level. Therefore, the local stress concentration appears in peripheral regions of hydrate decomposition. In the region without decomposition of hydrates, owing to pore pressure reduction, the effective stress increases. Under high stress conditions, hydrate regions and the surrounding formation undergo extrusion and deformation, reducing the porosity of the formation, as shown in Fig. 6d. It can be seen from the figure that the nephogram of the porosity distribution in hydrate decomposition regions is correlated with the nephogram of the porosity of hydrate saturation.

Stratum deformation process

In the hydrate decomposition process, as the reservoir near the wellbore is compacted, the corresponding deformation is bound to occur in other regions of the slope. Figure 7 shows the nephograms of the strains, plastic strains, and displacements of the submarine slope when the hydrate decomposition range is 250 m and the corresponding time is 1354 days. According to Fig. 7a, the distribution density of principal strains reflects the degree of change in strain in a region. The strain distribution consists of two mutually perpendicular arrows, the longer and the shorter of which represent the max. and min. principal strains respectively. Both the length and color stand the value of strain. The inward and outward directions of arrows represent the compressive and tensile stress respectively. It can be seen that in the hydrate sediments the increase of effective stress caused by depressurization and were dominated by the compressive effects. It is worth noting that the strain reached 0.06 in the hydrate decomposed area in the formation, which was the minimum value in all slope. After hydrate decomposition, the strength of the highly decomposed reservoirs was lower than that of the overlying strata, and the higher the decomposition degree is, the lower the strength; thus, the decomposed area was most compressed. By comparison, the underburden was the least influence caused by the hydrate

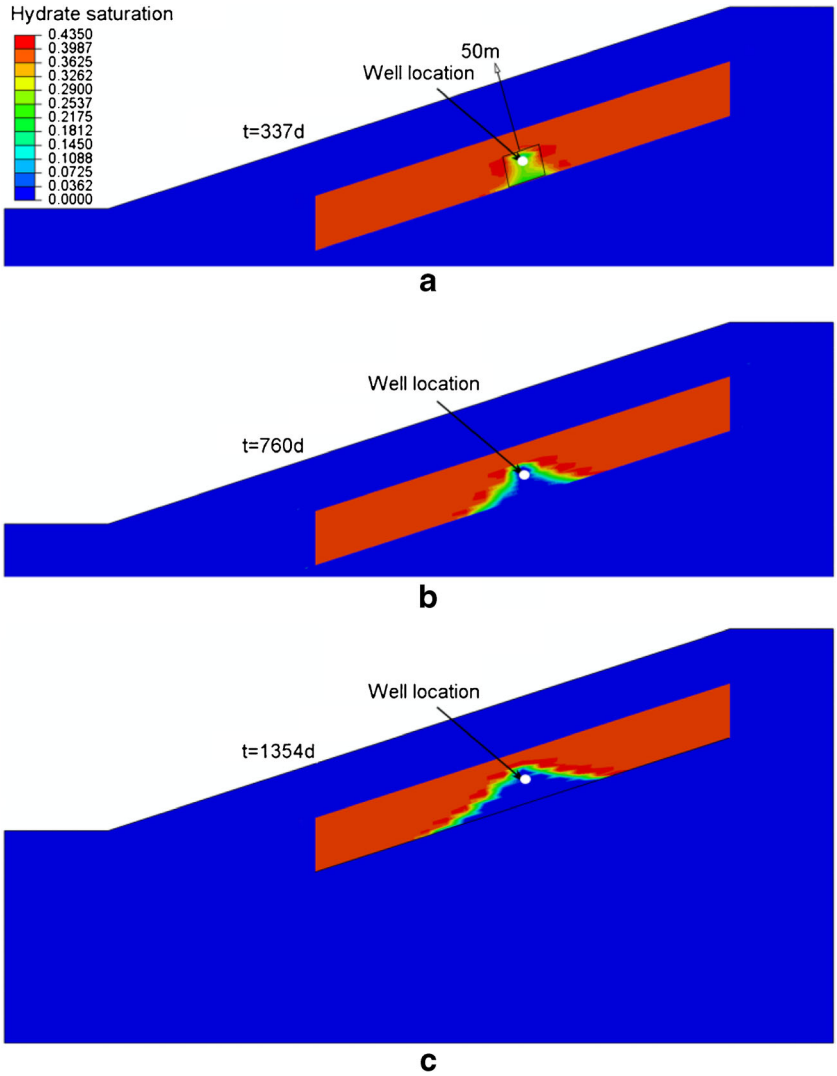

Fig. 5 Nephogram of distribution of hydrate saturation with different decomposition scales. **a** 50 m. **b** 150 m. **c** 250 m

dissociation while the sediment above the hydrate layer showed less strains, but the maximum tensile strain appeared here. Figure 7b shows the plastic strain distribution. The place where the tensile strain appeared also had the plastic strain while the other part of the stratum did not exhibit plastic deformation. It means that, in the hydrate dissociation process under the case-19, the shear failure across the whole slope was not induced, which suggests that the subsequent landslide would not be produced.

Combining with the Fig. 7c (the displacement distribution map), it can be seen that the central region of the hydrate decomposition zone settles downward, while the formations on both sides of the center slip to the central region of the hydrate decomposition zone. After migrating decomposition products (gas and water) through the shaft, cavities appear in the formation, and the lower formation is uplifted due to the extrusion of horizontal stress. According to the displacement directions, the displacement of the slope during mining process is dominated by the settlement, thus causing the corresponding formation slippage. Although the influenced scale is large, when the hydrate decomposition range is 250 m, the maximum resultant displacement of the slope is 2.441 m while the maximum settlement is 2.323 m. The ratio of the maximum settlement to the slope height is approximately 0.7% and the ratio of the maximum settlement to the hydrate thickness is approximately 2.3%. The values obtained through the simulation are similar to the simulation results of Jin et al. (JIn et al. 2018) and are very similar to the volume deformation after hydrate decomposition obtained by Gupta et al. (Gupta et al. 2015), demonstrating that the numerical model in this study is reliable. In addition, such a degree of deformation has some influence on construction safety and wellbore stability while not causing massive submarine geological disasters.

Figure 8a presents the curve of resultant displacement on the surface of the submarine slope after hydrate production for different times. At four time nodes, the corresponding hydrate decomposition ranges successively are 20 m, 50 m, 150 m, and 250 m. It can be seen from the figure that with the increase in time, the

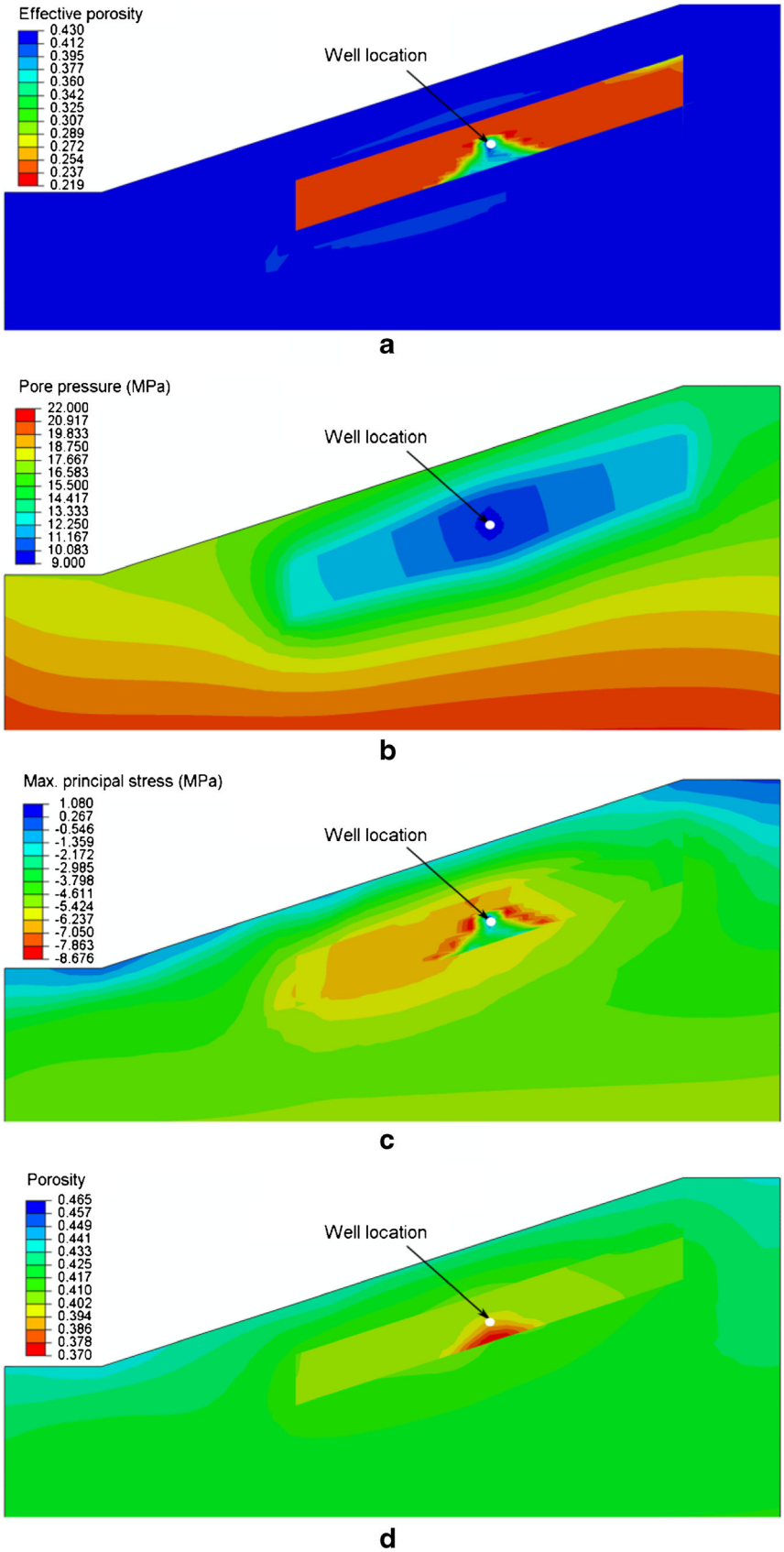

Fig. 6 Nephogram of formation parameters when hydrate decomposition range is 50 m. **a** Distribution of effective porosity. **b** Distribution of pore pressure. **c** Distribution of maximum principal stress. **d** Distribution of porosity

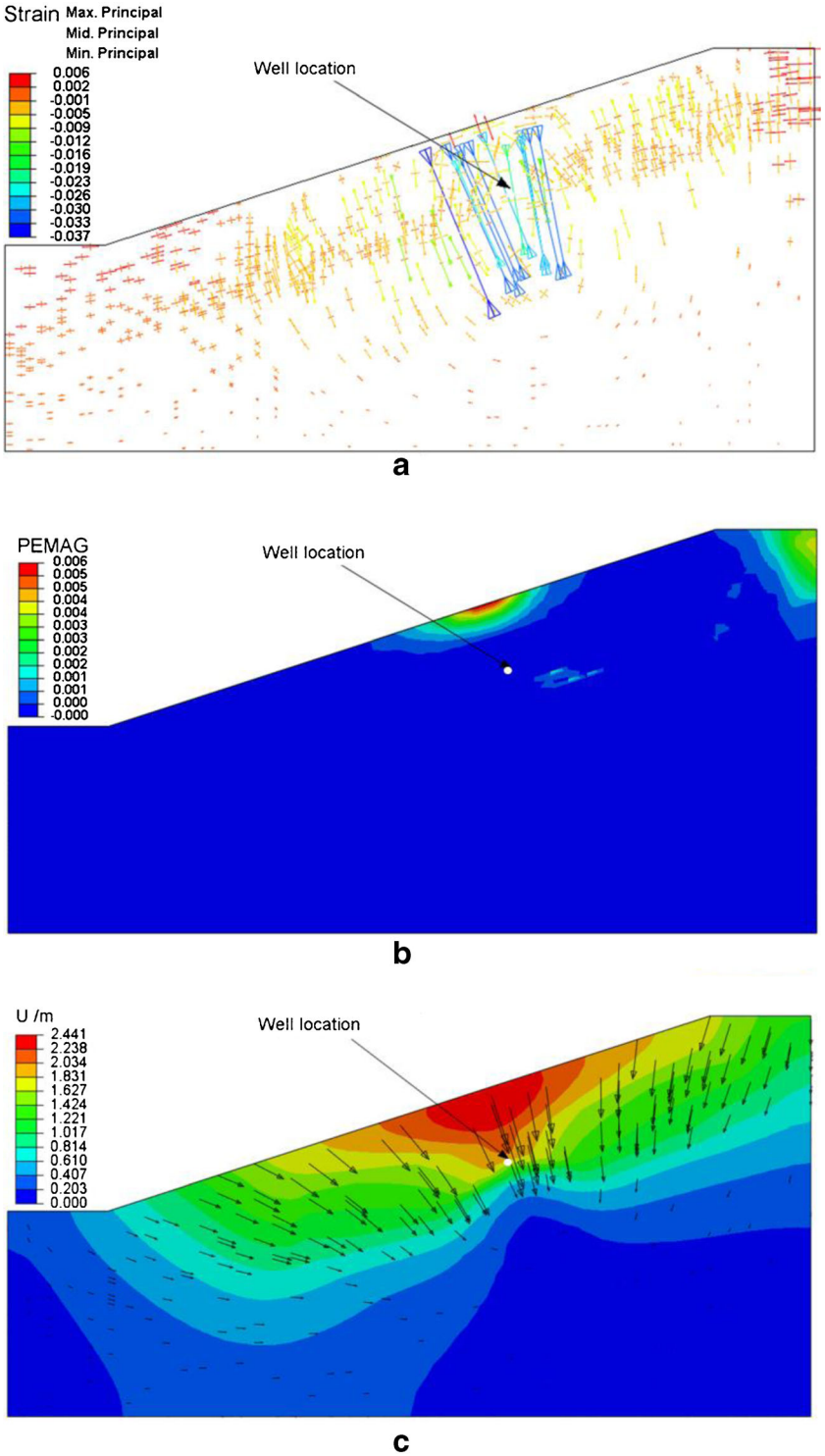

Fig. 7 Distribution of the slope under the hydrate decomposition range of 250 m. **a** Principal strains. **b** Plastic strain. **c** Displacement of magnitude

maximum displacement of the formation increases constantly, while the rate gradually decreases. During the hydrate recovery period, the corresponding maximum submarine settlement was approximately 1 m in 337 days of hydrate decomposition. When the hydrate decomposition time was 1359 days, the displacement reached approximately 2.3 m, indicating that settlement in the formation caused by hydrate decomposition reached a high level at an early stage, and then its growth rate gradually reduced with time. Obviously, as the hydrate decomposition degree went up, the value of submarine settlement had an increase. As shown in Fig.

7c, on the same projection surface which connected the maximum displacement point between the slope surface and the wellbore, the line was almost vertical to the slope surface. It indicates that the horizontal distance between the point which was directly above the wellbore on the slope surface and the point where the maximum displacement occurred was influenced by the slope angle, hydrate thickness, overburden thickness, and the well location. In addition, as presented in Fig. 8b, although the visible slope response was led by the settlement, the slope stability declined obviously with the hydrate decomposition.

Landslide development process

Slope instability mechanism

When the degree of hydrate decomposition met the requirements of experimental schemes, the hydrate decomposition analysis was terminated, and the strength reduction analysis starts to determine the safety factor of the slope and the potential landslide risks. Landslides caused by hydrate decomposition occurred in hydrate formations and overburden layers, while the underlying layers were less influenced. The load (including gravity, water pressure) on the slope remains unchanged while the strength of the whole slope reduced with the increase of reduction factor in the strength reduction analysis. Due to the changing of the stratum strength, the formation stress redistributed. Figure 9 a and b show the principal stress distribution under different reduction factor, 1.0618 and 1.348 respectively, and Fig. 9c shows the difference between Fig. 9a and b. It can be seen that, for most part of the slope, such as the underburden and the horizontal edge area, the principal stress changed slightly. It also shows that in the hydrate decomposition area the stress changed significantly in the reduction process. Specifically, the most complex principal distribution appeared in the decomposed front area while that in the totally decomposed area is simple due to its lowest strength (also can refer to Fig. 6c). These indicate that the failure of hydrate formation will occur under the effect of strength reduction method.

Figure 10a shows the shear strain distribution, and Fig. 10b shows the true principal strain distribution with the reduction factor 1.348. As shown in Fig. 10a, the maximum shear strain occurring in the hydrate decomposed area reached 0.616 while the maximum strain was 0.641 in Fig. 10b. Comparing Fig. 10 with Fig. 9c, the spatial consistency between the strain and stress can be obviously noticed. The shear strain from slope toe to the hydrate decomposed area was also consistent with the principal strain. The results indicate that the shear strain is in a dominant status in the total strain in the slope, which means that the shear-strain–based failure will occur in the formation and subsequent landslides will happen.

The manifestation of slope instability

The slope failure is described based on the development process of the plastic zone internal to slopes (Gravina et al. 2017). The presence of the plastic zone suggests that the skeleton structure of the formation starts to be damaged, while the formation of the plastic connection zone indicates that the formation begins to be unstable. The dynamic failure of the slopes in the reduction process is determined through the development of the plastic zone and corresponding displacements. As shown in Fig. 11, because the strength of the hydrate decomposition zone is significantly lower than that of the sedimentary layers, with the increase in the reduction factor, the hydrate decomposition zone enters the plastic yield stage firstly. In the stage of the emergence of the plastic zone, the slope basically inherits displacement characteristics in the hydrate decomposition stage and does not show obvious deformation. As the reduction factor constantly increases, the plastic zone develops to the toe and top of the slope by taking the hydrate decomposition zone as the center, thus forming a weak plastic connection zone. Under these conditions, the displacement characteristics of slope are different from those of the hydrate decomposition process. Specifically, the total displacement of the slope is converted to be dominated by displacement in the x-direction. Under the displacement in the horizontal direction, the left end of the slope lifts upward and the right end slips downward in the vertical direction.

With an increasing reduction factor, the scope of the plastic yield zone is increasingly expanded, and the degree of plastic deformation is aggravated to form a continuous plastic connection zone connecting the toe and top of the slope as well as the hydrate zone. Eventually, calculation ends due to misconvergence. In this step, the displacement is dominated by the sliding instead of the formation strength. As shown in Fig. 12, the overburden of the plastic connection zone was influenced by significant horizontal displacement. The largest horizontal displacement and the maximum displacement were generated near the wellbore. The directions of internal movement of the formation suggest that the sliding of slope along the failure surface causes the displacement of the formation. The toe area of the slope is affected by the sliding surface and will have an upward displacement. The final displacement under slope failure is as high as 42 m, and the submarine slope with hydrates undergoes a large-scale submarine landslide, running from the top to the toe of the slope under the decomposition effect of hydrates. In this case, the reduction factor is equivalent to the safety factor of the slope and can be applied to characterize the degree of stability of the slope.

Determination of the safety factor

The safety factor is the most important index in evaluating the slope stability and an ideal quantitative index in orthogonal analysis. As mentioned in "Slope instability criteria," there are several criteria in acquiring the safety factor. Based on the displacement at the bent point of the slope top, the formation of plastic penetration zone (according to Fig. 11b), and the nonconvergent calculation, the safety factors are shown in Fig. 13. Obviously, different criteria correspond to different safety factors, but the maximum error does not exceed 10% which is acceptable in engineering.

As shown in Fig. 13, when the calculation ended, the maximum Fs was acquired. It means that as long as the Fs acquired with this criterion is less than one, the landslide will happen definitely. Meanwhile, it is the most widely used criterion in finite element slope stability analysis for the unified evaluation criterion (Gupta et al., 2016; Maji, 2017). In the orthogonal analysis process, only the comparative analysis can obtain credible results. The first two evaluation criteria can only be based on the top node displacement curve in the calculation process or the plastic strain distribution, artificially selecting a certain reduction factor as the safety factor, which will introduce subjective errors in the comparative analysis. The third way of judging is to fix the minimum increment between

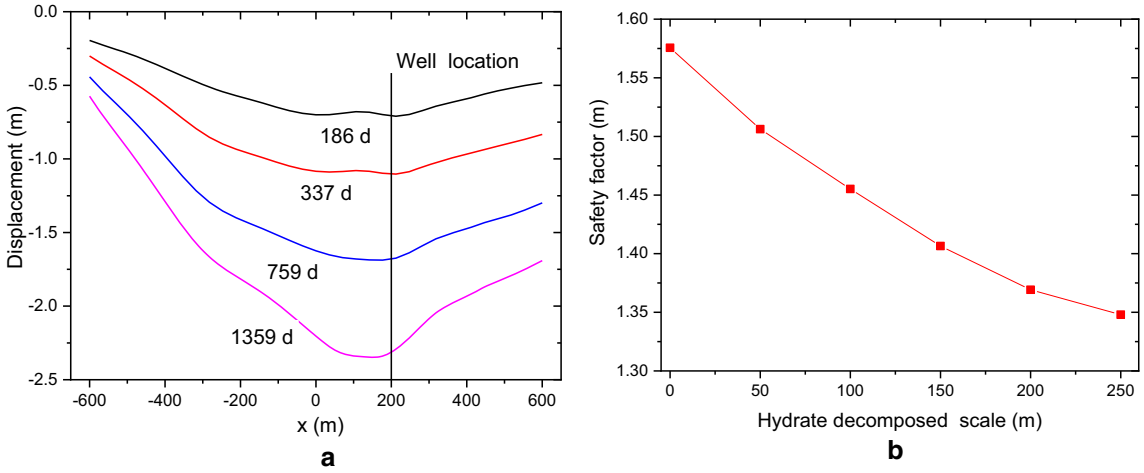

Fig. 8 **a** Submarine slope surface displacement. **b** Hydrate decomposition scale and safety factor curve

two iterations to form a unified evaluation standard. Therefore, this paper uses the calculation termination as the slope instability criterion and employs the safety factor to determine the slope stability.

Factors influence on slope stability

The safety factors of submarine slopes obtained through numerical simulation under different schemes are displayed in Fig. 14. In most cases, the safety factor is greater than one above the safety line. The safety factor of the submarine slope is closely related to the occurrence conditions and the hydrate decomposition range, in addition to diverse factors including the slope angle, slope strength, and seawater depth. Moreover, hydrate occurrence conditions and hydrate decomposition degree and slope conditions are likely to show a synergistic effect on slope stability. Thus, it is necessary to conduct an analysis on the synergistic effect of the two factors. Because the influence of the submarine slope angle on the safety factor of the slope is extremely significant, the error caused by the factor needs to be excluded. During analysis in the section, except for the analysis of the synergistic effect between the hydrate decomposition range and submarine slope angle, the slope angle is 18° when analyzing the synergistic effects between the other factors and the hydrate decomposition range.

Influence of slope angel

Figure 15 shows the influence curves of the slope angle on the safety factor of the slope with different hydrate decomposition degrees. It can be seen from the figure that with the growth of the slope angle, the safety factor of the slope speeds up to then decrease significantly. The reason for this result is that the shallow strata of the submarine sedimentary layer appear as weak cementitious strata, and there is low cohesion in the sedimentary layer. The slope stability depends on the fact that the frictional forces between particles can resist the component of gravity along the direction of the slope. With a growing slope angle, on the one hand, the component of gravity down the slope rapidly increases so that the frictional force is unable to counteract the gravity component. On the other hand, on the condition of having the same span length as the slope, the growth of the slope angle means an increasing height difference between the top and toe of the slope. As a result, the geostress on the toe of the slope along the horizontal direction increases significantly. Under the mutual effect of the two factors, the safety factor of the slope is rapidly reduced with the increasing slope angle.

The increase in the hydrate decomposition range can also greatly reduce the safety factor of the slope, and the reduction rate gradually increases with the growth of the degree of decomposition. The decomposed hydrate-containing formation synchronously loses the cementation and support effects of hydrates so that the strength of the stratum rapidly declines. As shown in the nephogram obtained through the numerical simulation, during the analysis of strength reduction, the hydrate decomposition zone is subjected to significant plastic strain. The larger the hydrate decomposition range is, the larger the scope of the plastic zone, the earlier the zone is where the hydrates are decomposed turns into the plastic yield stage and the easier the slope failure appears, which is reflected by the decreasing safety factor.

With the exploitation of hydrates, with the mutual effect between the hydrate decomposition range and slope angle, the stability of the submarine slope with hydrates is dramatically reduced, and its safety factor is significantly lower than one. This finding indicates that the slope with hydrates is likely to undergo a large-scale submarine landslide. Therefore, when exploiting hydrates in a slope with a large angle, it is necessary to fully assess the slope stability.

Influence of seawater depth

The figure shows the influence of seawater depth on the safety factors of slopes with different degrees of hydrate decomposition. As shown in Fig. 16, the growth of the seawater depth causes a slight increase in the safety factors of slopes. Compared with the influence of the hydrate decomposition range on the safety factor of the slopes, seawater depth showed a small influence on the safety factor, which was consistent with the research result obtained by Urlaub et al. (2013). Within the 400-m change range of the seawater depth, the mean increase in the safety factor with the same decomposition degree is approximately 0.03. Under natural conditions, the effective stress on the submarine strata mainly

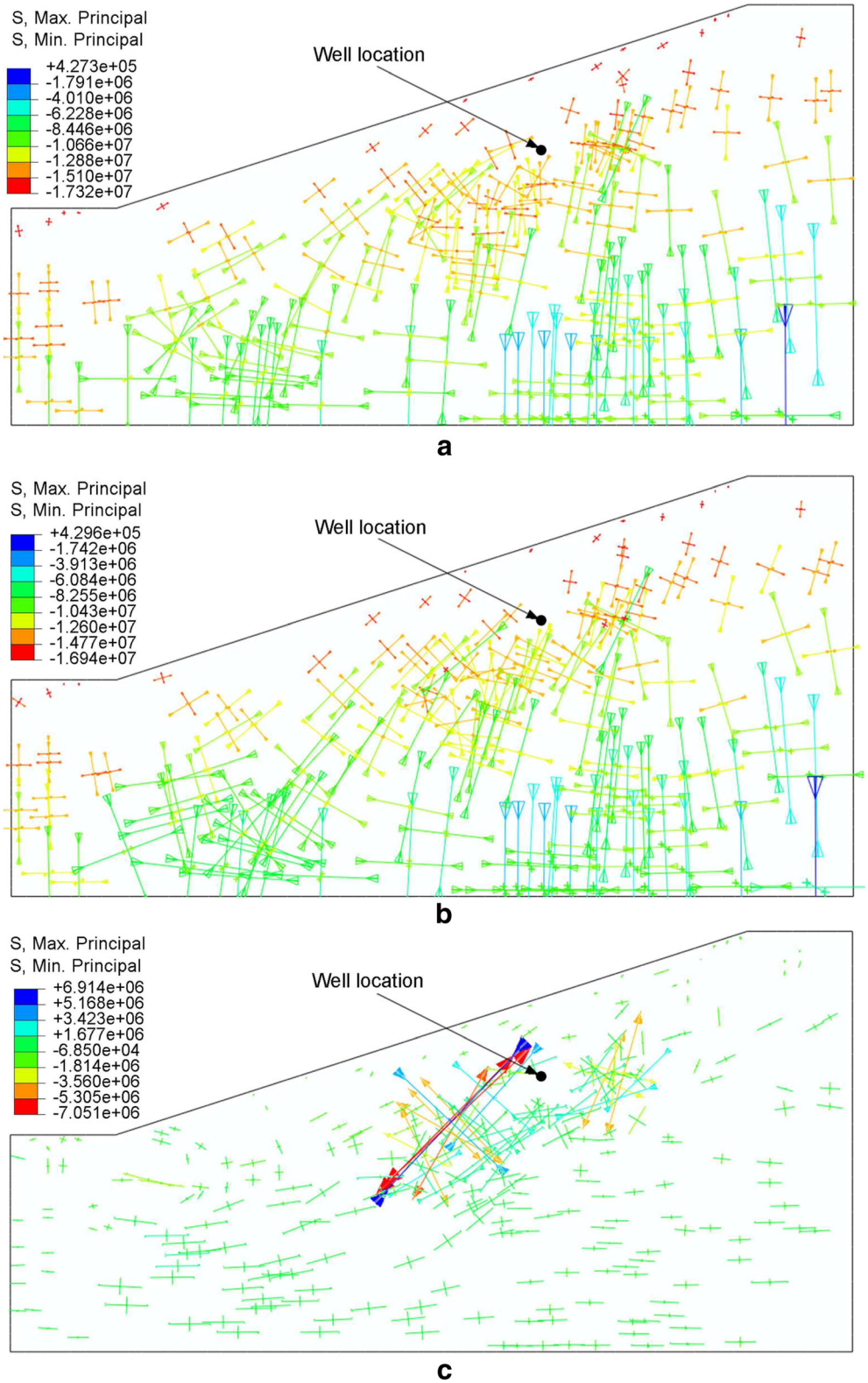

Fig. 9 The principal stress distribution. **a** The reduction factor is 1.0618. **b** The reduction factor is 1.3480. **c** The difference between Fig. 9a and b

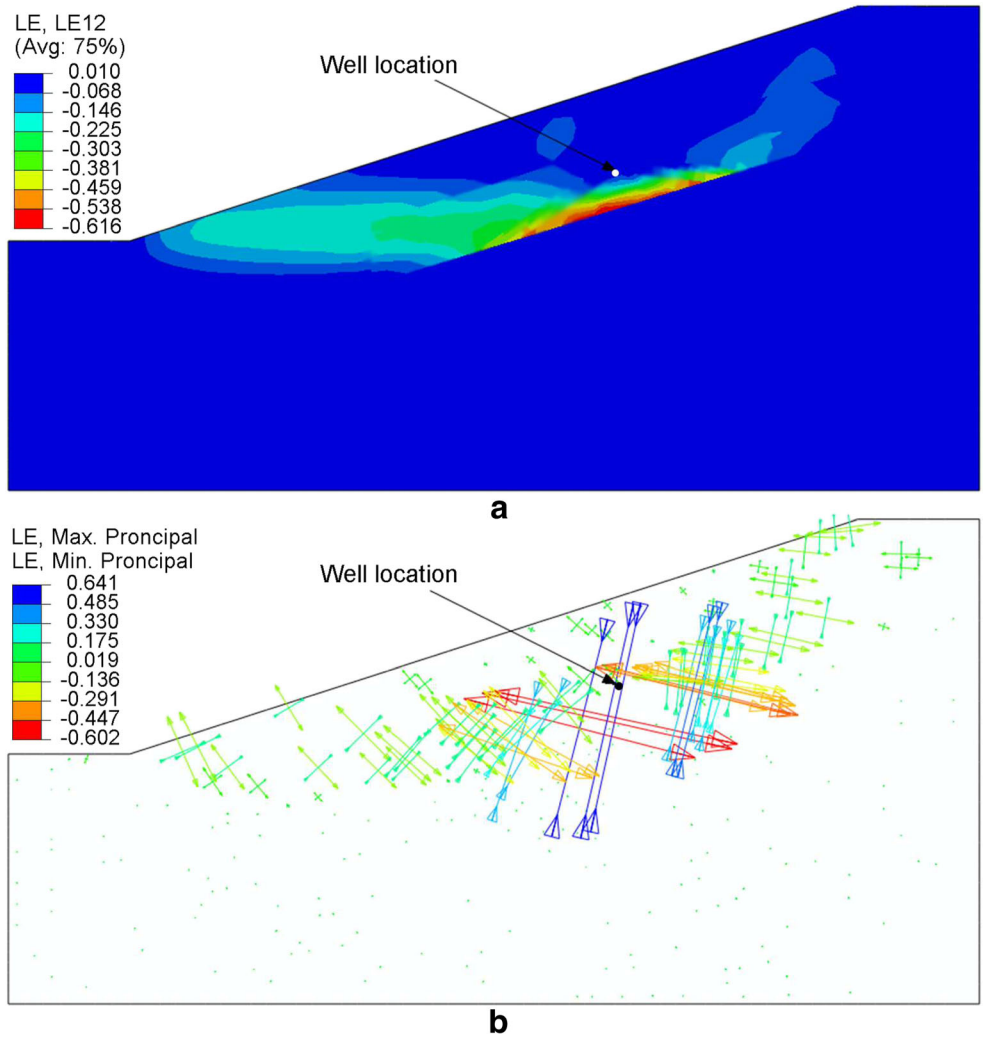

Fig. 10 Under the Fr 1.348, the distribution of **a** shear strain and **b** principal strains

depends on the depth of the strata with the sludge level and the density difference between the sedimentary layer and seawater, as well as the elastic coefficient of the pores. The effective stress coefficient of the sedimentary layer in the shallow part of deep water is approximately 0.97; thus, the increase in the seawater depth mainly influences the pore pressure of the strata and the pressure of overlying strata, causing only a slight growth in effective stress on the strata. The degree of stability of submarine slopes is mainly determined by the effective stress on the strata, and increasing the effective stress is conducive to maintaining the stability of the submarine slope. Therefore, the curve regarding the safety factor shows such a change law: slight increases with increasing seawater depth. During the excavation of hydrates by using a depressurization production, the solid hydrates are decomposed into water and natural gas. The high pore pressure of the strata due to a high seawater depth inhibits the expansion of gas produced in hydrate decomposition to thus reduce the disturbance of decomposition products to the structure of reservoirs to some extent. From this perspective, during production, the stability of the submarine slopes can increase to a certain degree with increasing seawater depth in the area where the hydrate reservoir occurs. However, the increased degree of stability of submarine slopes contributed by the effect is significantly lower than the reduction degree of the stability of submarine slopes induced by reduced hydrate strength due to hydrate decomposition (Liu, et al., 2009). Therefore, under a decomposition scale of certain hydrates, with increasing seawater depth, the safety factor of the slope increases slightly. Additionally, the stability of the submarine slope declines greatly with the increase in the hydrate decomposition range.

Influence of hydrate overburden depth

Figure 17 shows the influence of the overburden depth of hydrates on the safety factor of the slope with different degrees of decomposition. On the condition that hydrates are not decomposed, the safety factor decreases slightly with the increasing overburden depth of hydrates. In this case, the strength of the hydrate layer in the strata is larger than the strength of the sedimentary layer itself. The safety factor of the

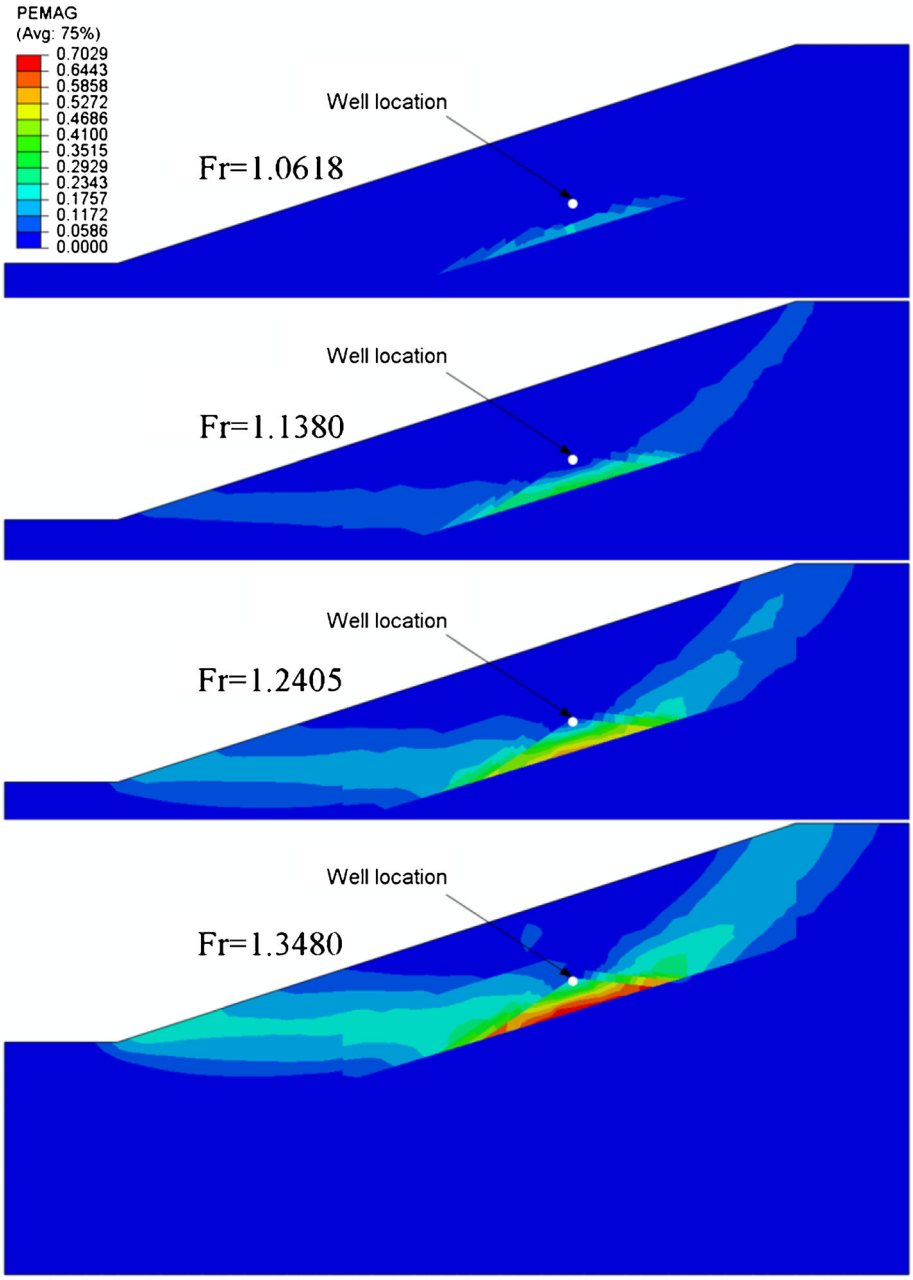

Fig. 11 Magnitude plastic strain distribution responding to different reduction factors

slope is determined by the strength of the sedimentary layer itself. The hydrate zone is equivalent to a slightly hard interlayer, which has a supportive effect on the slope stability. Because slope failure generally happens in shallow parts, the shallower the overburden depth of the hydrates is, the more possible the factor promotes the slope stability.

After the decomposition of hydrates, the larger the overburden depth of the hydrates is, the higher the safety factor of the slope. When the overburden depth of the hydrates reaches 250 m, the safety factor tends to be stable. The possible reason for this result is that, after the hydrates are decomposed, the strength of the zone greatly declines. The zone where hydrates are decomposed is basically considered the lower limit of the range of slope failure, and the overlying strata of the hydrate layer are all subjected to settlement or slippage. Due to the increase in the thickness of the overlying strata, the scale of slope failure increases. The more energies that are needed for failure, the larger the resistance to failure triggered by the strength reduction of the hydrate zone in the lower part is. Thus, the safety factor of the slope gradually increases.

Overall, the reduction in reservoir strength caused by hydrate decomposition dominantly controls the safety factor. The higher the hydrate decomposition range is, the larger the rise amplitude

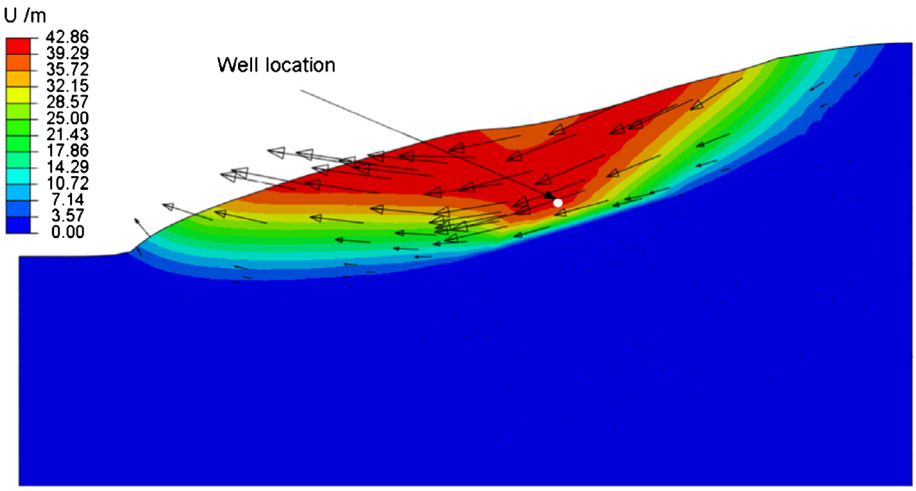

Fig. 12 Displacement distribution of strata and the displacement vector arrows when calculation ended

of the safety factor induced by the increase in the overburden depth of the hydrates. Until the failure of the slope occurs, the overlying strata of the hydrates are not subjected to significant plastic deformation during analysis. When the large-scale plastic deformation effect of the zone where hydrates are decomposed is applied on the overlying strata, the overlying strata show a buffer action similar to a spring. When hydrates are buried at a shallow part and decomposed on a large scale, an insufficient buffer area exists between the hydrate layer and the sea floor. Therefore, a small action range aggravates the degree of influence of the zone, which results in a decrease in the strength of the decomposed zone and great deformation from the top of the hydrate layer to the sea floor. With the effects of the above two aspects, the slope stability is weakened. In contrast, when hydrates are buried in a deep part, a large propagation and buffer scope appear during the deformation of the zone where the hydrates are decomposed, resulting in the growth of the safety factor of the slope. Additionally, the larger the hydrate decomposition range is, the more significant the effect. Therefore, the exploitation of hydrates at a shallow part is extremely beneficial to subsequent risk prevention.

Influence of hydrate layer thickness

Figure 18 displays the change curve of the safety factor of slopes with the thickness of hydrate layers of different degrees of decomposition. On the condition that hydrates are not decomposed, the safety factor of the slope increases slightly with the growth in the thickness of the reservoir. Similar to the influence law of overburden depth of hydrates on the safety factor of slopes, although slope failure depends on the strength of the sedimentary layer, a high-strength hydrate layer still can slightly promote the stability of submarine strata. Once the hydrates are decomposed, with the increase in the thickness of the hydrates, the safety factor of the slopes gradually decreases, and the reduction rate gradually slows down. Obviously, with the same hydrate decomposition range, the

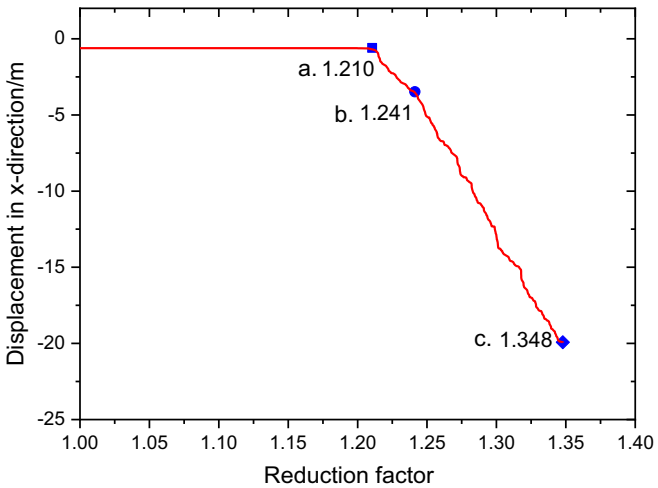

Fig. 13 Different safety factors under different criteria. **a** Displacement at the bent point of the slope top. **b** The formation of plastic penetration zone. **c** The nonconvergent calculation

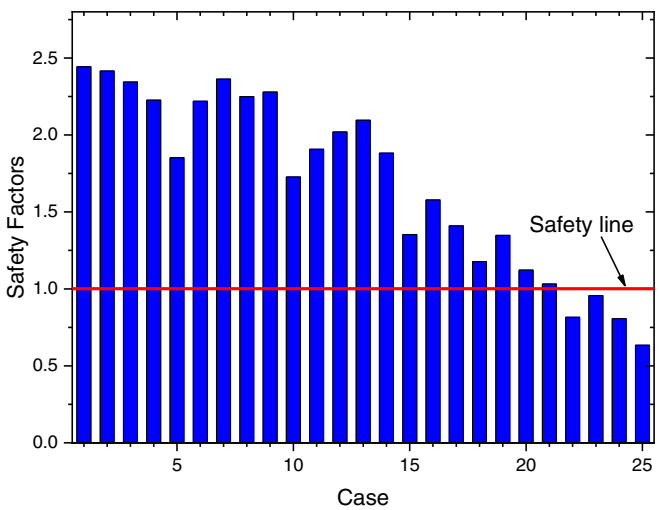

Fig. 14 Safety factors in different cases

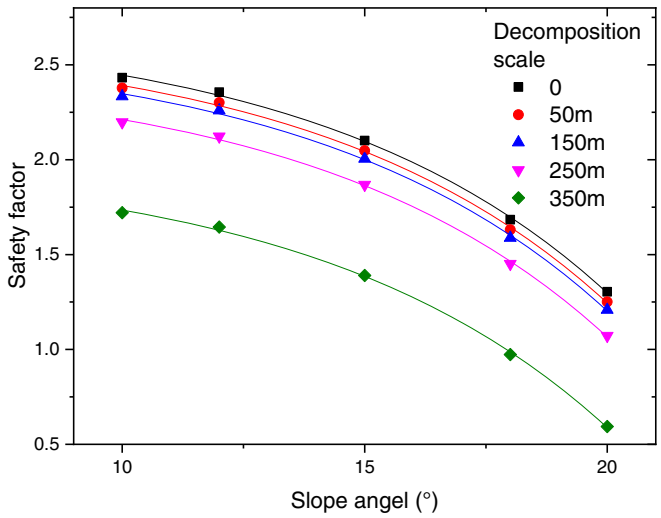

Fig. 15 The influence of slope angle on the safety factor of the slope

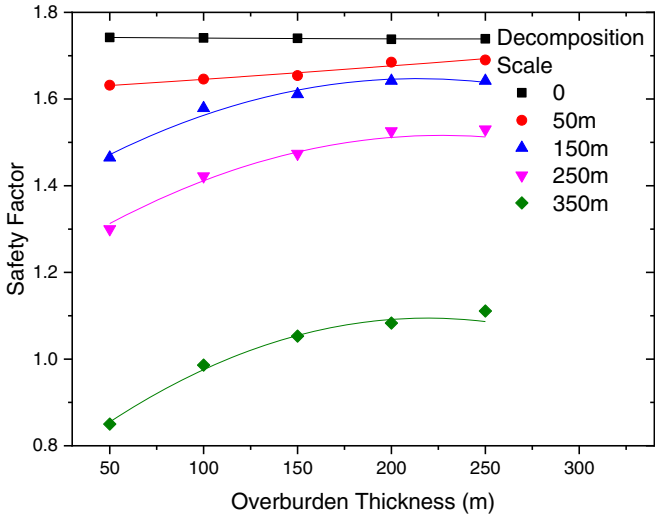

Fig. 17 The influence of overburden depth of hydrates on safety factor of slopes

increase in the thickness of hydrates implies the growth of the volume of the zone where hydrates are decomposed. The larger the effective pore volume caused by the decomposition of hydrates is, the larger the scope of the low-strength zone and the less favorable the slope stability. With the increasing thickness of the hydrate layers, the reduction rate of the safety factor of the slope decreases, which is possibly caused by the increase in the scope of the failure of the whole slope.

With the growth of the hydrate decomposition range, the reduction amplitude of the curve of the safety factor with the changing thickness of the hydrates increases, and the reduction rate accelerates, indicating that the influences of decomposition degree and the thickness of hydrates on slope stability show not only a superposition effect but also an interactive effect, that is, with the synergistic effect of the two factors, the slope stability reduces dramatically, implying that although the exploitation of a thick hydrate layer can bring significant gas production and benefit, there is a high potential geological risk.

Influence of initial hydrate saturation

Figure 19 shows the relationship curve between the initial saturation of the hydrate layers and the safety factor of the slopes with different hydrate decomposition degrees. On the condition that hydrates are not decomposed, the curve of the safety factor of slopes appears approximately as a horizontal line. The reason for this result is similar to that of the aforementioned analysis. When hydrates are decomposed at a certain degree, the safety factor shows an approximately linear reduction, with increasing saturation within the research scope. With an increasing hydrate decomposition range, the reduction amplitude of the safety factor increases, and the reduction rate also increases. Through the analysis, it can be seen that the phenomenon occurs mainly

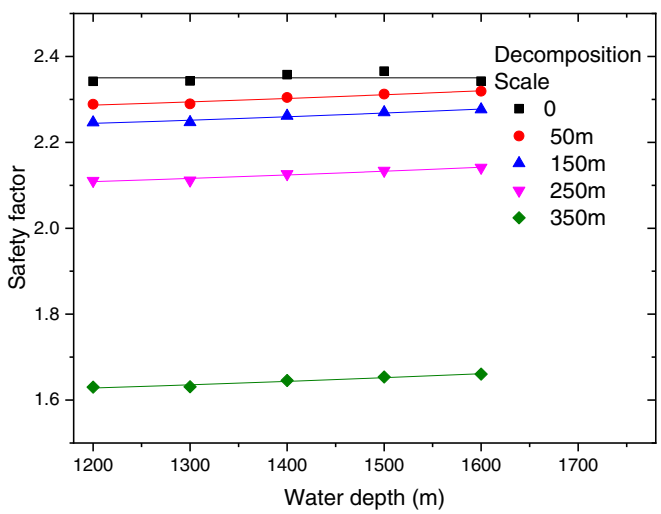

Fig. 16 The influence of seawater depth on safety factor of slope

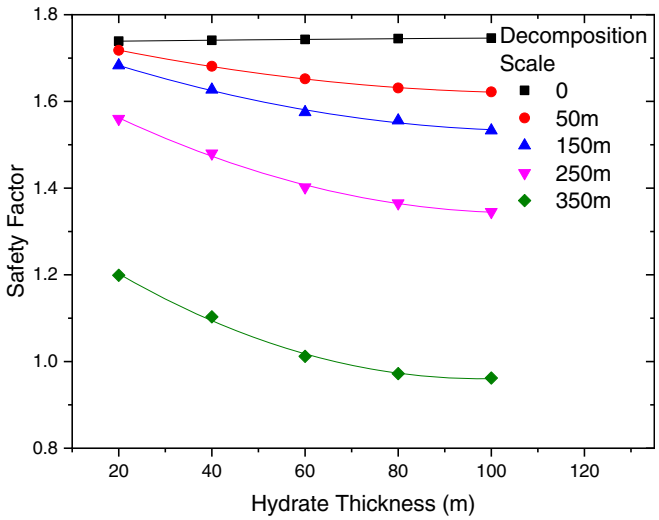

Fig. 18 The influence of the thickness of hydrate layers on safety factor of slopes

because of two aspects. On the one hand, the higher the initial saturation of hydrates is, the greater the products obtained after decomposition of hydrates, the larger the void volume of the strata afterwards, and the less favorable the stability of the strata. On the other hand, the model supposes that the strength of the strata is related only to the saturation of the hydrates; thus, the strengths of the strata after the decomposition of hydrates are basically the same. The higher the initial saturation of hydrates is, the larger the reduction amplitude of the strength of the strata between before the decomposition and after the decomposition, and the larger the strength difference between the zones where hydrates are and are not decomposed. This outcome easily triggers the stress concentration and is also unfavorable for the stability of the strata. With the aforementioned effect and the interactive effect between saturation and the hydrate decomposition range, the safety factor of submarine slopes is lower than one, implying that there is also a significant risk of submarine landslides with a high saturation of hydrates.

Sensitivity analysis of factors for submarine slope stability

Figure 20 shows the range analysis of factors influencing the stability of submarine slopes. Figure 20a presents the distribution of the statistics of safety factors under various conditions. As shown in the figure, the distribution of the statistics of safety factors under various influence conditions approximately reflects the influence trends and degrees of various factors on the slope stability. For example, the growth of the slope angle results in the large reduction of the safety factor. In contrast, seawater depth nonsignificantly impacts the safety factor of slopes. The influence of significant single factor or multifactor synergistic effects on slope stability needs to be characterized by the estimated marginal mean. The distribution result through the range analysis reflects the degrees of influence of various factors on the failure of submarine slopes. It can be seen from the sensitivity evaluation of each factor in Fig. 20b that the significance order of the factors affecting the stability of the seabed slope is the slope angle, the range of hydrate decomposition, the hydrate thickness, the hydrate overburden depth, the hydrate saturation, and the seawater depth. Among them, the influence of seawater depth on the safety factor is significantly lower than other factors.

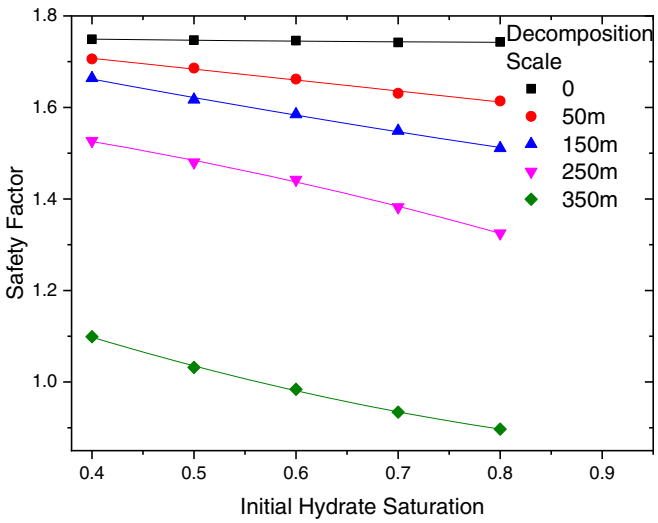

Fig. 19 The influence of the initial saturation of a hydrate layer on safety factor of slopes

Based on the aforementioned analysis, the significance levels of the other factors (except for seawater depth) that influence the safety factors were tested. The test was carried out by using III-sum of squares in SPSS software, and the calculated results and significance levels are shown in the table. The sums of squares and mean squares in the table reflect the effects of various factors on the indexes. On the condition of taking the significance level of 0.01, when the significance was larger than 0.01, it was inferred that the factor had no significant influence on the safety factor of the slopes. Otherwise, the factor influenced the safety factor of slopes. And the lower the significance value is, the more significant the influence of the factor. After analyzing Table 4, the obtained result was similar to the result obtained through the range analysis, that is, the influence of the slope angle on the safety factor was substantially higher than that of the other factors. The hydrate decomposition range showed a highly significant influence on the safety factor of the slopes. The influences of the initial saturation, overburden depth, and thickness of hydrates on the safety factor of slopes were of the same magnitude.

Conclusion

By using numerical simulation, the process of submarine settlements and landslides induced by hydrate decomposition was described based on an orthogonal experimental design and the strength reduction method. Furthermore, the influence laws of various factors on the stability of submarine slopes were systematically analyzed. By doing so, the following conclusions are drawn.

1. On the condition that the slope angle is lower than 15°, hydrates can cause the submarine settlement and slippage of the submarine sedimentary level to the mining center but fail to trigger a submarine landslide. When the slope angle is more than 15°, it is necessary to evaluate the stability of submarine slopes during the production process of hydrates. When the submarine slope angle is larger than 18°, there is a large risk of triggering a large-scale submarine landslide on the condition that the leading edge of the decomposition of the hydrates is approximately 150 m away from the mine.
2. Among the explored factors, according to the significance level that influences the stability of submarine slopes, the factors are displayed in a descending order as follows: the submarine slope angle, hydrate decomposition range, thickness of hydrate layers, overburden depth of hydrates, initial hydrate saturation, and seawater depth, where the seawater depth nonsignificantly influences the stability of the submarine slopes.
3. With the increase in the submarine slope angle, the stability of the submarine slopes accelerates to reduction; likewise, the growth of the hydrate decomposition range can also significantly decrease the slope stability, while the increasing overburden depth of the hydrate layers is favorable for increasing the slope stability. Moreover, the increase in the thickness and initial saturation of the hydrate layers can greatly reduce the slope when

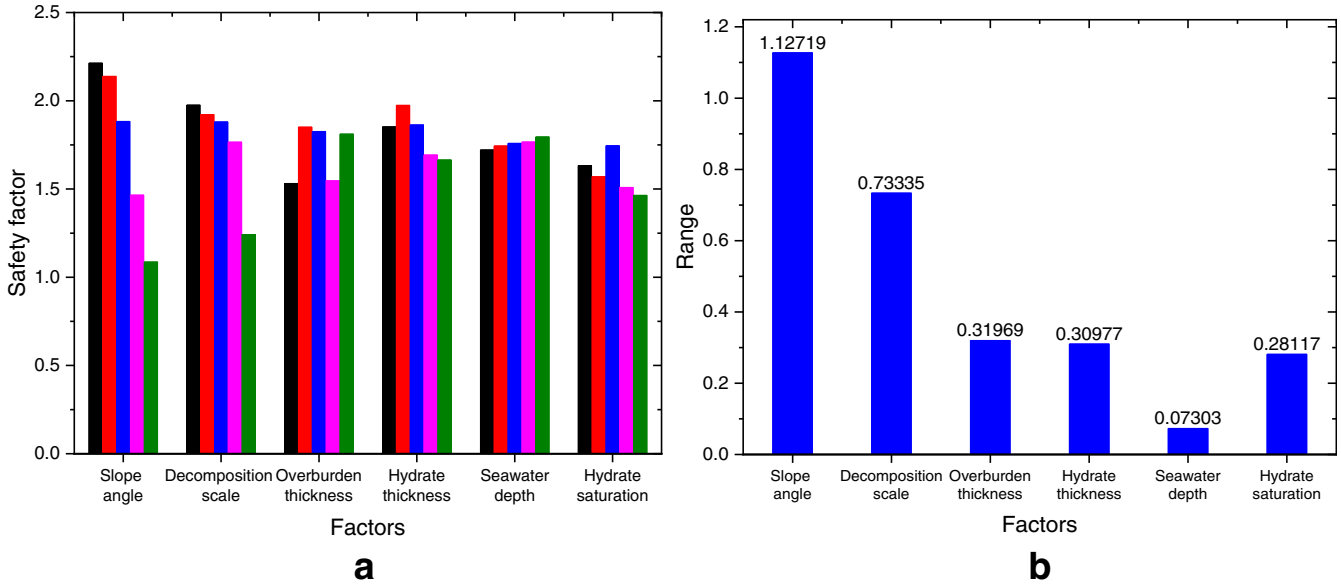

Fig. 20 Range analysis on various factors influencing the stability of submarine slope. **a** Distribution of statistics of safety factors under various factors. **b** Sensitivity evaluation on influence degrees of various factors

combined with the effect of the hydrate decomposition range. The growth of seawater depth slightly increases the slope stability.

Funding informationThis work is supported by the Qingdao National Laboratory for Marine Science and Technology (QNLM2016ORP0212), the National Natural Science Foundation Project of China (51704311), Program for the Changjiang Scholars and Innovative Research Team in University (IRT_14R58), the Fundamental Research Funds for the Central Universities, National Key Research and Development Program (Grant No. 2016YFC0304005), and the National Basic Research Program of China (973 Program) (Grant No. 2015CB251201).

Appendix. Multifield coupling model in porous media

ABAQUS can solve the heat flow-solid-stress field coupling in porous media. Based on the principle of effective stress, the constitutive behavior of each phase in the porous medium is analyzed by discretizing the porous medium. According to the continuity equation, the deformation behavior of each phase is coupled with the thermal behavior. The following are the key solutions. The detailed solution process can be found in the ABAQUS 2016 Documentation.

The effective stress principle for porous media is as follows:

$$\overline{\sigma}^{*} = (1-n_t)\overline{\sigma} - n_t\overline{p_t}\mathbf{I}$$

$$n_t \overset{def}{=} \frac{dV_t}{dV}$$

1. Discretized equilibrium statement for a porous medium

Equilibrium is expressed by writing the principle of virtual work for the volume under consideration in its current configuration at time t:

$$\int_V \boldsymbol{\sigma} : \delta\boldsymbol{\epsilon} dV = \int_S t\cdot\delta\boldsymbol{v} dS + \int_V \boldsymbol{f}\cdot\delta\boldsymbol{v} dV + \int_V (sn + n_t)\rho_w \boldsymbol{g}\cdot\delta\boldsymbol{v} dV$$

where f are all body forces except the weight of the wetting liquid.

The virtual velocity field is interpolated by

$$\delta\boldsymbol{v} = N^N \delta v^N$$

where $N^N(S_i)$ are interpolation functions defined with respect to material coordinates, S_i.

Table 4 Test on inter-subject effect

Factors	Type III sum of squares	Degree of freedom	Mean square	F	Significance
Slope angel	4.520	4	1.130	1106.348	0.000011
Decomposition scale	1.528	4	0.382	373.888	0.00061
Overburden thickness	0.093	4	0.023	22.734	0.005
Hydrate thickness	0.078	4	0.020	19.196	0.007
Hydrate saturation	0.070	4	0.018	17.168	0.009

The virtual rate of deformation is interpolated as

$$\delta\varepsilon = \beta^N \delta v^N$$

where, in the simplest case,

$$\beta^N = sym\left(\frac{\partial \delta N^N}{\partial x}\right)$$

Although, more general forms are used in some of the elements in ABAQUS. The virtual work equation is thus discretized as follows:

$$\delta v^N \int_V \beta^N : \sigma dV = \delta v^N \left[\int_S N^N \cdot t dS + \int_V N^N \cdot f \delta v dV + \int_V (sn + n_t)\rho_w N^N \cdot g dV\right]$$

2. Constitutive behavior in a porous medium

Liquid response:

For the liquid in the system (the free liquid in the voids and the entrapped liquid), we assume the following:

$$\frac{\rho_w}{\rho_w^o} \approx 1 + \frac{u_w}{K_w} - \varepsilon_w^{th}$$

where ρ_w is the density of the liquid, ρ_w^o is its density in the reference configuration, $K_w(\theta)$ is the liquid's bulk modulus, and

$$\varepsilon_w^{th} = 3\alpha_w(\theta - \theta_w^o) - 3\alpha_w|_{\theta^I}(\theta^I - \theta_w^o)$$

is the volumetric expansion of the liquid caused by the temperature change. Here, $\alpha_w(\theta)$ is the thermal expansion coefficient of the liquid, θ is the current temperature, θ^I is the initial temperature at this point in the medium, and θ_w^o is the reference temperature for thermal expansion. Both ${}^{u}/_{K_w}$ and ε_w^{th} are assumed to be small.

Solid response:

The solid matter in the porous medium is assumed to have the local mechanical response under pressure:

$$\frac{\rho_g}{\rho_g^o} \approx 1 + \frac{1}{K_g}\left(su_w + \frac{\bar{p}}{1 - n - n_t}\right) - \varepsilon_g^{th}$$

where $K_g(\theta)$ is the bulk modulus of this solid matter, s is the saturation in the wetting fluid, and

$$\varepsilon_g^{th} = 3\alpha_g\left(\theta - \theta_g^o\right) - 3\alpha_g\Big|_{\theta^I}\left(\theta^I - \theta_g^o\right)$$

is its volumetric thermal strain. Here, $\alpha_g(\theta)$ is the thermal expansion coefficient for the solid matter, and θ_g^o is the reference temperature for this expansion; $1 - \rho_g/\rho_g^o$ is assumed to be small.

3. Continuity statement for the wetting liquid phase in a porous medium

The total mass of wetting liquid in the control volume is

$$\int_V \rho_w [dV_w + dV_t] = \int_V \rho_w (n_w + n_t) dV$$

where ρ_w is the mass density of the liquid.

The time rate of change of this mass of wetting liquid is

$$\frac{d}{dt}\left[\int_V \rho_w (n_w + n_t) dV\right] = \int_V \frac{1}{J}\frac{d}{dt}(J\rho_w (n_w + n_t)) dV$$

Constitutive behavior:

Introducing the flow constitutive law allows the mass continuity equation to be written:

$$\int_V \left[\delta u_w \left(\left(\frac{\rho_w}{\rho_w^o}(sn + n_t)\right) - \frac{1}{J}\left(\frac{\rho_w}{\rho_w^o} J(sn + n_t)\right)_t\right) + t\frac{k_s}{\rho_w^o\left(1 + \beta\sqrt{\mathbf{v}_w \cdot \mathbf{v}_w}\right)}\frac{\partial \delta u_w}{\partial \mathbf{x}} \cdot \mathbf{k} \cdot \left(\frac{\partial \delta u_w}{\partial \mathbf{x}} - \rho_w g\right)\right] dV \quad t\int_S \delta u_w \frac{\rho_w}{\rho_w^o} sn\mathbf{n} \cdot \mathbf{v}_w dS = 0$$

Volumetric strain in the liquid and grains:

$$\frac{\rho_w}{\rho_w^o} n \approx 1 - \frac{1}{J}\left(1 - n^o - n_t^o + h_t\right) + \frac{\bar{p}}{K_g} + u_w\left(\frac{1}{K_w} + \frac{1 - n^o - n_t^o}{J}\left(\frac{1}{K_g} - \frac{1}{K_w}\right)\right) - \varepsilon_w^{th} + \frac{1}{J}\left(1 - n^o - n_t^o\right)\left(\varepsilon_w^{th} - \varepsilon_g^{th}\right)$$

4. Solution strategy for coupled diffusion/deformation

The coupled system of equations to be solved is as follows:

$$K^{MN}\bar{c}_\delta^N - L^{MP}\bar{c}_u^P = P^M - I^M$$

and pore fluid flow:

$$-\left(B^{MQ}\right)^{T}\bar{c}_{\delta}^{M}- \quad tH^{QP}\bar{c}_{u}^{P}=R^{Q}$$

where

$$R^{Q}= \quad t\left[-Q_{t+\quad t}^{Q}+\left(\widehat{B}^{MQ}\right)^{T}\bar{v}_{t+\Delta t}^{M}+\widehat{H}^{QP}\bar{u}_{t+\Delta t}^{P}\right]$$

5. Heat transfer solution

Energy balance: The basic energy balance is as follows:

$$\int_{V}\rho\dot{U}dV=\int_{S}qdS+\int_{V}rdV$$

This relationship is usually written in terms of a specific heat, neglecting the coupling between mechanical and thermal problems:

$$c(\theta)=\frac{dU}{d\theta}$$

Heat conduction is assumed to be governed by the Fourier law,

$$\mathbf{f}=-\mathbf{k}\frac{\partial\theta}{\partial x}$$

Boundary conditions can be specified as prescribed temperature, $\theta=\theta(x,t)$.

Spatial discretization

A variational statement of the energy balance, together with the Fourier law, is obtained directly by the standard Galerkin approach as follows:

$$\int_{V}\rho\dot{U}\delta\theta dV+\int_{V}\frac{\partial\delta\theta}{\partial\mathbf{x}}\bullet\mathbf{k}\bullet\frac{\partial\theta}{\partial\mathbf{x}}=\int_{V}\delta\theta rdV+\int_{S_q}\delta\theta qdS$$

The thermal equilibrium equation for a continuum in which a fluid is flowing with velocity **v** is as follows:

$$\int\delta\theta\left[\rho c\left(\frac{\partial\theta}{\partial t}+\mathbf{v}\frac{\partial\theta}{\partial\mathbf{x}}\right)-\frac{\partial}{\partial\mathbf{x}}\bullet\left(\mathbf{k}\bullet\frac{\partial\theta}{\partial\mathbf{x}}\right)-q\right]dV+\int_{S_q}\delta\theta\left[\mathbf{n}\bullet\mathbf{k}\bullet\frac{\partial\theta}{\partial\mathbf{x}}-q_s\right]dS=0$$

References

Almenningen S, Flatlandsmo J, Fernø MA, Ersland G (2016, April) Production of sedimentary methane hydrates by depressurization. In: SPE Bergen One Day Seminar. Society of Petroleum Engineers

Althuwaynee OF, Asikoglu O, Eris E (2018) Threshold contour production of rainfall intensity that induces landslides in susceptible regions of northern Turkey. Landslides 15(8):1541–1560

Bhade P, Phirani J (2015) Gas production from layered methane hydrate reservoirs. Energy, 82, 686-696. Chen X, Zhang X, Lu X, Wei W, Shi Y (2016). Numerical study on the deformation of soil stratum and vertical wells with gas hydrate dissociation. Acta Mech Sinica 32(5):905-914

Bondevik S, Stormo SK, Skjerdal G (2012) Green mosses date the Storegga tsunami to the chilliest decades of the 8.2 ka cold event. Quat Sci Rev 45:1–6

Bru G, Fernández-Merodo JA, García-Davalillo JC, Herrera G, Fernández J (2018) Site scale modeling of slow-moving landslides, a 3D viscoplastic finite element modeling approach. Landslides 15(2):257–272

Chen XP, Zhu HH, Huang JW, Liu D (2016) Stability analysis of an ancient landslide considering shear strength reduction behavior of slip zone soil. Landslides 13(1):173–181

Chen L, Feng Y, Kogawa T, Okajima J, Komiya A, Maruyama S (2018a) Construction and simulation of reservoir scale layered model for production and utilization of methane hydrate: the case of Nankai Trough Japan. Energy 143:128–140

Chen L, Feng Y, Okajima J, Komiya A, Maruyama S (2018b) Production behavior and numerical analysis for 2017 methane hydrate extraction test of Shenhu, South China Sea. J Nat Gas Sci Eng 53:55–66

Chong ZR, Yin Z, Tan JHC, Linga P (2017) Experimental investigations on energy recovery from water-saturated hydrate bearing sediments via depressurization approach. Appl Energy 204:1513–1525

De Luca DL, Versace P (2017) A comprehensive framework for empirical modeling of landslides induced by rainfall: the Generalized FLaIR Model (GFM). Landslides 14(3):1009–1030

Feng JC, Wang Y, Li XS, Li G, Zhang Y, Chen ZY (2015) Production performance of gas hydrate accumulation at the GMGS2-Site 16 of the Pearl River Mouth Basin in the South China Sea. J Nat Gas Sci Eng 27:306–320

Feng XT, Zhao J, Zhang X, Kong R (2018) A novel true triaxial apparatus for studying the time-dependent behaviour of hard rocks under high stress. Rock Mech Rock Eng:1–15

Gravina T, Figliozzi E, Mari N, Schinosa FDLT (2017) Landslide risk perception in Frosinone (Lazio, Central Italy). Landslides 14(4):1419–1429

Gulbrandsen AC, Svartås TM (2017) Effects of PVCap on gas hydrate dissociation kinetics and the thermodynamic stability of the hydrates. Energy Fuel 31(9):9863–9873

Guo T, Qu Z, Gong D, Lei X, Liu M (2016) Numerical simulation of directional propagation of hydraulic fracture guided by vertical multi-radial boreholes. J Nat Gas Sci Eng 35:175–188

Gupta S, Helmig R, Wohlmuth B (2015) Non-isothermal, multi-phase, multi-component flows through deformable methane hydrate reservoirs. Comput Geosci 19(5):1063–1088

Gupta V, Bhasin RK, Kaynia AM, Kumar V, Saini AS, Tandon RS, Pabst T (2016) Finite element analysis of failed slope by shear strength reduction technique: a case study for Surabhi Resort Landslide, Mussoorie township, Garhwal Himalaya. Geomatics, Natural Hazards and Risk 7(5):1677–1690

Hu Y, Lee BR, Sum AK (2017) Insight into increased stability of methane hydrates at high pressure from phase equilibrium data and molecular structure. Fluid Phase Equilib 450:24–29

Hunt, J. E. (2012). Determining the provenance, recurrence, magnitudes and failure mechanisms of submarine landslides from the Moroccan Margin and Canary Islands using distal turbidite records (Doctoral dissertation, University of Southampton)

Jin G, Xu T, Xin X, Wei M, Liu C (2016) Numerical evaluation of the methane production from unconfined gas hydrate-bearing sediment by thermal stimulation and depressurization in Shenhu area, South China Sea. J Nat Gas Sci Eng 33:497–508

Jin G, Lei H, Xu T, Xin X, Yuan Y, Xia Y, Juo J (2018) Simulated geomechanical responses to marine methane hydrate recovery using horizontal wells in the Shenhu area, South China Sea. Mar Pet Geol 92:424–436

Kamath, V. A. (1998). A perspective on gas production from hydrates. In JNOC's Methane Hydrate Intl. Symposium, Chiba City, Japan (pp. 20–22)

Katagiri J, Konno Y, Yoneda J, Tenma N (2017) Pore-scale modeling of flow in particle packs containing grain-coating and pore-filling hydrates: verification of a Kozeny–Carman-based permeability reduction model. J Nat Gas Sci Eng 45:537–551

Kostov N, Ning J, Gosavi SV, Gupta P, Kulkarni K, Sanz P (2015) Advanced drilling induced fracture modeling for wellbore integrity prediction. In: SPE Annual Technical Conference and Exhibition. Society of Petroleum Engineers

Kukowski N, Greinert J, Henrys S (2010) Morphometric and critical taper analysis of the Rock Garden region, Hikurangi Margin, New Zealand: implications for slope stability and potential tsunami generation. Mar Geol 272(1–4):141–153

Lee SY, Holder GD (2001) Methane hydrates potential as a future energy source. Fuel Process Technol 71(1–3):181–186

Li G, Moridis GJ, Zhang K, Li XS (2010) Evaluation of gas production potential from marine gas hydrate deposits in Shenhu area of South China Sea. Energy Fuel 24(11):6018-6033

Li X, Jaffal H, Feng Y, El Mohtar C, Gray KE (2018) Wellbore breakouts: Mohr-Coulomb plastic rock deformation, fluid seepage, and time-dependent mudcake buildup. J Nat Gas Sci Eng 52:515–528

Lin JS, Seol Y, Choi JH (2017) Geomechanical modeling of hydrate-bearing sediments during dissociation under shear. Int J Numer Anal Methods Geomech 41(14):1523–1538

Ling K, Wu X, Zhang H, He J (2014) Improved gas resource calculation using modified material balance for overpressure gas reservoirs. J Nat Gas Sci Eng 17:71–81

Maji VB (2017) An insight into slope stability using strength reduction technique. J Geol Soc India 89(1):77–81

Maslin M, Vilela C, Mikkelsen N, Grootes P (2005) Causes of catastrophic sediment failures of the Amazon Fan. Quat Sci Rev 24(20):2180–2193

Masson DG, Arzola RG, Wynn RB, Hunt JE, Weaver PPE (2011) Seismic triggering of landslides and turbidity currents offshore Portugal. Geochem Geophys Geosyst 12(12)

Micallef A, Mountjoy JJ, Canals M, Lastras G (2012) Deep-seated bedrock landslides and submarine canyon evolution in an active tectonic margin: Cook Strait, New Zealand. In: Submarine mass movements and their consequences. Springer, Dordrecht, pp 201–212

Miyazaki K, Masui A, Sakamoto Y, Aoki K, Tenma N, Yamaguchi T (2011) Triaxial compressive properties of artificial methane-hydrate-bearing sediment. J Geophys Res: Solid Earth (B6):116

Miyazaki K, Tenma N, Aoki K, Yamaguchi T (2012) A nonlinear elastic model for triaxial compressive properties of artificial methane-hydrate-bearing sediment samples. Energies 5(10):4057–4075

Moridis GJ (2002) Numerical studies of gas production from methane hydrates. In: SPE Gas Technology Symposium. Society of Petroleum Engineers

Moridis GJ, Kowalsky MB, Pruess K (2007) Depressurization-induced gas production from class-1 hydrate deposits. SPE Reserv Eval Eng 10(05):458–481

Moridis, G. J., Reagan, M. T., & Zhang, K. (2008). The use of horizontal wells in gas production from hydrate accumulations

Mountjoy JJ, Micallef A (2012) Polyphase emplacement of a 30 km 3 blocky debris avalanche and its role in slope-gully development. In: Submarine mass movements and their consequences. Springer, Dordrecht, pp 213–222

Mountjoy JJ, McKean J, Barnes PM, Pettinga JR (2009) Terrestrial-style slow-moving earthflow kinematics in a submarine landslide complex. Mar Geol 267(3–4):114–127

Nair VC, Prasad SK, Kumar R, Sangwai JS (2018) Energy recovery from simulated clayey gas hydrate reservoir using depressurization by constant rate gas release, thermal stimulation and their combinations. Appl Energy 225:755–768

Pedley KL, Barnes PM, Pettinga JR, Lewis KB (2010) Seafloor structural geomorphic evolution of the accretionary frontal wedge in response to seamount subduction, Poverty Indentation, New Zealand. Mar Geol 270(1–4):119–138

Pinkert S, Grozic JLH (2014) Prediction of the mechanical response of hydrate-bearing sands. J Geophys Res: Solid Earth 119(6):4695–4707

Sánchez M, Gai X, Santamarina JC (2017) A constitutive mechanical model for gas hydrate bearing sediments incorporating inelastic mechanisms. Comput Geotech 84:28-46

Soldi M, Guarracino L, Jougnot D (2017) A simple hysteretic constitutive model for unsaturated flow. Transp Porous Media 120(2):271–285

Su Z, Moridis GJ, Zhang K, Wu N (2012) A huff-and-puff production of gas hydrate deposits in Shenhu area of South China Sea through a vertical well. J Pet Sci Eng 86:54–61

Sultan N (2007) Comment on "Excess pore pressure resulting from methane hydrate dissociation in marine sediments: a theoretical approach" by Wenyue Xu and Leonid N. Germanovich. J Geophys Res: Solid Earth 112(B2)

Sultan N, Garziglia S (2011) Geomechanical constitutive modelling of gas-hydrate-bearing sediments. In: The 7th International Conference on Gas Hydrates (ICGH 2011)

Sultan N, Cochonat P, Foucher JP, Mienert J (2004) Effect of gas hydrates melting on seafloor slope instability. Mar Geol 213(1–4):379–401

Sun X, Mohanty KK (2006) Kinetic simulation of methane hydrate formation and dissociation in porous media. Chem Eng Sci 61(11):3476–3495

Urlaub M, Talling PJ, Masson DG (2013) Timing and frequency of large submarine landslides: implications for understanding triggers and future geohazard. Quat Sci Rev 72:63–82

Wang Z, Yu J, Zhang J, Liu S, Gao Y, Xiang H, Sun B (2019) Improved thermal model considering hydrate formation and deposition in gas-dominated systems with free water. Fuel 236:870–879

Wei J, Cheng Y, Yan C, Li Q, Zou D, Zhang H (2019) Drilling parameter optimizing strategies to prevent hydrate decomposition risks. Appl Therm Eng 146:405–412

White MD, Wurstner SK, McGrail BP (2011) Numerical studies of methane production from class 1 gas hydrate accumulations enhanced with carbon dioxide injection. Mar Pet Geol 28(2):546–560

Wien K, Kölling M, Schulz HD (2007) Age models for the Cape Blanc debris flow and the Mauritania slide complex in the Atlantic Ocean off NW Africa. Quat Sci Rev 26(19–21):2558–2573

Xu W, Germanovich LN (2006) Excess pore pressure resulting from methane hydrate dissociation in marine sediments: a theoretical approach. J Geophys Res: Solid Earth (B1):111

Yamamoto K (2015) Overview and introduction: pressure core-sampling and analyses in the 2012–2013 MH21 offshore test of gas production from methane hydrates in the eastern Nankai Trough. Mar Pet Geol 66:296–309

Yamamoto K, Dallimore S (2008) Aurora-JOGMEC-NRCan Mallik 2006-2008 gas hydrate research project progress. Natural Gas Oil 304:285–4541

Yamamoto, K. Terao, Y. Fujii, T. Ikawa, T. Seki, M. Matsuzawa, M. & Kanno, T. (2014, May). Operational overview of the first offshore production test of methane hydrates in the Eastern Nankai Trough. In Offshore Technology Conference. Offshore Technology Conference

Yan C, Cheng Y, Li M, Han Z, Zhang H, Li Q, Teng F, Ding J (2017) Mechanical experiments and constitutive model of natural gas hydrate reservoirs. Int J Hydrog Energy 42(31):19810–19818

Yan C, Li Y, Cheng Y, Wang W, Song B, Deng F, Feng Y (2018) Sand production evaluation during gas production from natural gas hydrates. J Nat Gas Sci Eng 57:77–88

Zhang K, Moridis GJ, Wu N, Li X, & Reagan MT (2010) Evaluation of alternative horizontal well designs for gas production from hydrate deposits in the Shenhu Area, South China Sea. In International oil and gas conference and exhibition in China. Society of Petroleum Engineers

Zhou S, Zhao J, Li Q, Chen W, Zhou J, Wei N, Guo P, Sun W (2018) Optimal design of the engineering parameters for the first global trial production of marine natural gas hydrates through solid fluidization. Nat Gas Industry B 5(2):118–131

Zhu H, Zhao X, Guo J, Jin X, An F, Wang Y, Lai X (2015) Coupled flow-stress-damage simulation of deviated-wellbore fracturing in hard-rock. J Nat Gas Sci Eng 26:711–724

B. Song · Y. Cheng · C. Yan (✉) · Z. Han · J. Ding · Y. Li · J. Wei
Department of Petroleum Engineering,
China University of Petroleum (East China),
Qingdao, 266580, People's Republic of China
Email: yanchuanliang@163.com